UNITED STATES ATOMIC ENERGY COMMISSION

AECD-3486

EFFECT OF SHAPE AND MATERIAL ON THE THERMAL RUPTURE OF CERAMICS

By
E. M. Baroody
W. H. Duckworth
E. M. Simons
H. Z. Schofield

May 22, 1951

Battelle Memorial Institute

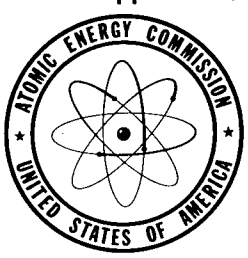

Technical Information Service, Oak Ridge, Tennessee

METALLURGY AND CERAMICS

In the interest of economy, this report has been reproduced direct from copy as submitted to the Technical Information Service.

PRINTED IN USA
PRICE 35 CENTS
Available from the
Office of Technical Services
Department of Commerce
Washington 25, D. C.

Other issues of this report may bear the number BMI-70.

Work performed under
Contract No. W-7405-eng-92.

Date Declassified: January 21, 1953.

AEC, Oak Ridge, Tenn.-W30856

TABLE OF CONTENTS

TABLE OF CONTENTS (Continued)

SUMMARY

This report describes the first phase of an investigation of the effect of shape and material on the thermal rupture of ceramics. It deals primarily with thermal rupture caused by steady-state radial heat flow through a circular tube. One objective of this research is to ascertain under what conditions the heat flow per unit length causing failure, Q_{max}, can be written as the product of two factors: M, characterizing the material, and S, characterizing the shape of the specimen.

Dimensional analysis indicates that $Q_{max} = MS$, provided:

1. The material behaves according to Hooke's law.
2. Poisson's ratio may be considered a universal constant.
3. The material parameters, such as thermal conductivity, expansion coefficient, strength, and Young's modulus, are independent of temperature.
4. The boundary conditions are such as to introduce no additional variables, such as emissivity, heat-transfer coefficient, etc.

Mathematical expressions for M and S are presented for the case of steady-state radial heat flow from an external source through the wall of a circular tube. It was found that the magnitude of S depends upon the length-diameter ratio, h/b, as well as on the ratio of outer and inner radii, b/a. This was corroborated experimentally by tests with sintered ruby tubes of the same radius ratio but different lengths. The shortest tube withstood the greatest heat flow per unit length, as predicted. These tests were carried out in a thermal-rupture apparatus in which heat

from a graphite resistor rod passes outward through the walls of a cylindrical specimen surrounding the rod. Thermal stresses are increased by increasing the power to the heater rod, in small increments, until fracture occurs.

Consideration was given to the fact that M would be expected to vary with specimen temperature, since some of the material parameters in the expression for M are known to be temperature sensitive. Although tests to determine this temperature dependence of M for the bodies in question are planned, no experimental data are available at present. Hence, this effect was estimated from the effect of temperature on the contributing physical properties, and thermal-rupture data were corrected to the same temperature for comparison purposes.

In a brief series of thermal-rupture tests on beryllia tubes of the same intermediate length but different radius ratios, measured values of Q_{max}, corrected to the same length-diameter ratio, h/b, and the same outer wall temperature, increased with decreasing radius ratio, b/a, in much the same fashion as the theoretical value of S increases for the indefinitely thin washer. This would indicate that b/a enters the expression for S in approximately the same way for intermediate lengths as it does for extremely short tubes, although considerably more evidence would be required to establish this point conclusively. One item of special interest in these tests was the ability of thin-walled tubes to withstand the maximum power available, although analyses indicated that they should fracture. This phenomenom was explained by pyroplastic flow, which permitted relaxation of the thermal stresses under the conditions attained in these particular specimens.

It should be pointed out that the information presented in this report is preliminary in nature. Detailed equations for only the specialized cases of very short and of very long, round tubes are presented, and these are subject to certain restricted boundary conditions and assumptions. No theoretical analyses were made of intermediate-length tubes, which are, in fact, the most practical. Furthermore, no studies have been included for shapes other than circular tubes, or for the pertinent case of internal heat generation.

INTRODUCTION

Owing to their refractory nature, certain ceramic materials appear to have considerable promise as fuel-element materials, moderators, or structural members for high-temperature nuclear reactors. One major shortcoming, however, is their generally poor resistance to fracture from thermal stresses.

Thus, it is important that some reliable criterion be established to predict the ability of a given ceramic reactor component to withstand the thermal stresses in service. Such a criterion has been suggested.* Based on thermoelastic theory for heated round tubes, the maximum heat throughput before thermal rupture occurs might be expressed as the simple product of two factors as follows:

$$Q_{max} = MS .$$

Here, M is a parameter which depends only on the physical properties of the material and is called the material factor. S is a factor which

* MonN-383, pp. 203-207, September 15, 1947.

depends only on the shape of the body and is called the shape factor. If this concept is valid, then it should be possible to obtain values of M for all the materials of interest and values of S for all the shapes of interest and to combine the appropriate ones to predict the service behavior of any given material and shape.

It was felt, however, that a great deal of theoretical and experimental work would be required to evaluate the tenability of $Q_{max} = MS$ as a general performance index. Consequently, an investigation was begun at Battelle to study the validity of this product relationship, its limitations, methods of determining M and S, and factors influencing M and S.

The work described in this report is preliminary in nature and deals primarily with steady-state radial heat flow through the wall of a circular tube. Considerably more study and experimentation will be required before definite conclusions can be drawn about material and shape factors for the conditions pertinent to actual reactors.

THEORY AND BACKGROUND

General Considerations for Steady-State Conditions

In the present phase of this investigation, the maximum power per unit length which can be passed through the wall of a hollow circular cylinder without causing failure has been measured. In later phases of the program, specimens with non-circular cross section will be included, and heat will be produced internally and removed at the free surfaces. In all the work, the axial flow of heat is to be kept at a minimum. To plan and interpret such experiments, and to present their results in a

form convenient for consideration of reactor design, it is important to have some theoretical framework, even though this is incomplete, and in some degree tentative.

Some of the theoretical ideas and relationships now available are presented here, and in appendices at the end of the report. Emphasis is on steady-state conditions, which were maintained in nearly all the experimental work to date. Transient heating will be discussed in later reports. All quantitative relations developed or quoted assume elastic behavior of the body. It is recognized that plastic flow can be of great importance, and that in certain cases it is responsible for large differences between the predictions of elasticity theory and actual behavior.

In earlier work* on the evaluation of fuel elements in respect to thermal stress, it was pointed out that under certain conditions the power per unit length causing failure, Q_{max}, can be written as the product of two factors: M, characterizing the material, and S, characterizing the shape of the specimen. It is important to learn more about the conditions under which this simple product relationship can be used, and what can conveniently replace it in more complicated situations. A consideration of the calculation of thermal stresses in the elastic range is helpful in this connection.

One formulation of the appropriate thermoelastic equations is given in Appendix A, where they are applied to the problem of thermal stresses in a short circular cylinder. Here we consider what conclusions can be drawn regarding the variables determining Q_{max} without actually

---

* MonN-383, pp. 203-207, September 15, 1947.

solving these equations. The basic assumption in the analysis is that rupture occurs when some unspecified quantity of the dimensions of stress reaches a critical value, P. The temperature dependence of such quantities as thermal conductivity, coefficient of expansion, etc., is neglected. In addition, some statement must be made regarding boundary conditions. Those chosen at the start will be such as to lead to the simple product for Q_{max}. It will be evident, however, that with other, and possibly more interesting, boundary conditions, the arguments given will break down, and the validity of the original simple result will become very questionable.

The arguments are to cover both internal and external heating. In the internal-heating case, a cylinder of any cross section is considered and the boundary condition first assumed is that all the free surfaces are maintained at the same temperature. For external heating, consideration is limited to a cylinder whose cross section is a doubly connected area. It is then assumed that each of the two separate bounding surfaces is at its own uniform temperature. The difference between these two temperatures is determined if the power transferred per unit length of the cylinder is fixed, so that in calculating a temperature distribution corresponding to a given Q only one temperature needs to be specified to complete the boundary conditions. In neither of these cases does the value of the arbitrary boundary temperature influence the thermal stresses corresponding to a given power per unit length. For an unconstrained body, these stresses are determined by temperature differences, rather than by actual temperatures. Thus, these special boundary conditions introduce no variables which have to be considered in a dimensional analysis. It

is to be expected, then, that Q_{max} will be a function of the following variables, appearing in the thermoelastic equations, or describing the geometry of the specimen:

K = thermal conductivity,

α = coefficient of linear expansion,

E = Young's modulus,

ν = Poisson's ratio,

X = some linear dimension of the cylinder fixing its size,

P = "critical stress",

$S_1, S_2, \cdots S_m$ = dimensionless parameters fixing the shape of the specimen.

From these variables (including Q_{max} itself), the following dimensionless combinations may be formed:

$$\frac{Q_{max}\alpha}{K}, \frac{P}{E}, \nu, S_1, S_2, \cdots S_m .$$

It is then to be expected that the first of these is some function, say ϕ, of all the others, so that:

$$Q_{max} = \frac{K}{\alpha} \phi \left(P/E, \nu, S_1, S_2, \cdots S_m \right) . \qquad (1)$$

However, the argument may be carried beyond this point by giving attention to the pattern of the equations for calculating thermal stresses. In reality the calculation divides into: (1) the determination of the temperature distribution, and (2) the calculation of stresses from this distribution. Examination of the equations for (2) shows that any stress which arises entirely from the noncompatibility of the strains directly caused by some temperature distribution is a function of the shape

parameters and of ν, multiplied by $E\alpha\bar{T}$, where $\bar{T}$ is a quantity of the dimensions of temperature, to be calculated from the temperature distribution alone. For the boundary conditions discussed above, this $\bar{T}$ is Q/K multiplied by a function of the shape parameters alone. These considerations lead to:

$$Q_{max} = \frac{KP}{\alpha E} S\left(S_1, S_2, \ldots S_m, \nu\right) . \qquad (2)$$

Strictly speaking, this result does not permit us to think of Q_{max} as a product of material and shape factors, since the material parameter, ν, appears in the function S along with the shape parameters. However, ν is a quantity which does not vary very much from material to material, while some of the quantities of the factor $KP/\alpha E$ do vary a great deal. This encourages the hope that, to a useful approximation, ν may be regarded as a universal constant. To this approximation, Equation (2) is:

$$Q_{max} = MS , \qquad (3)$$

where:

$$M = \frac{KP}{\alpha E} ,$$

characterizes the material of the cylindrical specimen, and

$$S\left(S_1, S_2, S_3 \ldots S_M, \nu\right) ,$$

characterizes its shape.*

---

* We note that within the limits of the above analysis Q_{max} is independent of specimen size. In a case where the heat removed is generated internally, the maximum average power density might be of special interest. This is proportional to $\frac{Q_{max}}{X^2}$; that is, it varies inversely as the square of the length which fixes the scale of the specimen.

The arguments outlined above depend on the particular boundary conditions contemplated, and no longer apply in other cases. For example, suppose the surfaces from which heat is removed are actually radiating to cool surroundings. A new dimensional constant, appearing in the expression for the radiating power of the surface, now enters the calculation of the temperature distribution, and with it the possibility of an additional dimensionless combination involving Q_{max}. The validity of the product relation for Q_{max} then becomes very questionable, unless the problem has cylindrical symmetry. In this latter case, the temperature of the radiating surface will in fact be uniform, the new dimensional constant will not enter the problem, and the conclusions reached above continue to apply.

In the preceding discussion, the temperature dependence of such material parameters as thermal conductivity, the expansion coefficient, etc., has been ignored. When this variation is taken into account, a small deviation from the product relation for Q_{max} is to be expected. A calculation of this effect for a long hollow cylinder, heated at the inner surface, is given in Appendix B, and indicates that the deviation is indeed small. However, the questions of boundary conditions, and of the role of Poisson's ratio, present more serious difficulties and warn against considering the product relation as very general or very precise.

The Circular Cylinder (Steady State, External Heating)

In this section some well-known relations for thermal stresses in circular cylinders will be summarized.* These help towards understanding

* Calculations leading to these relations are given in §§ 113 and 114 of "Theory of Elasticity", S. Timoshenko (McGraw-Hill Book Company, New York, 1934).

of the experimental results to be given later in the report, and also illustrate some of the points which were made in the preceding, more general discussion. Consider first a very short circular cylinder with radii a and b, and height $2h$ with $b > a \gg h$. If a purely radial heat flow is maintained in the cylinder, the power per unit length crossing the wall being Q, the temperature is:

$$T(r) = \frac{Q}{2\pi K} \log \frac{b}{r} + T_b \quad . \tag{4}$$

The maximum tensile stress is the circumferential stress at the outer wall:

$$\sigma_\theta (b) = E\alpha (\bar{T} - T_b) \quad , \tag{5}$$

where $\bar{T}$ is the temperature averaged over the cross section of the wall. Inserting this average:

$$\sigma_\theta (b) = \frac{QE\alpha}{4\pi K} \left(1 - \frac{2a^2}{b^2 - a^2} \log \frac{b}{a} \right) \quad . \tag{6}$$

If failure occurs when this stress reaches the critical value, P, we have:

$$Q_{max} = MS \quad , \tag{7}$$

where:

$$M = PK/E\alpha \quad , \tag{8}$$

and:

$$S = 4\pi / \left(1 - \frac{2a^2}{b^2 - a^2} \log \frac{b}{a} \right) \quad . \tag{9}$$

Next consider a very long cylinder lying between the planes $z = \pm h$ with $h \gg b > a$. The maximum tensile stress is now expected to be a circumferential stress at the outer wall and at the end of the cylinder:

$$\sigma_\theta (b, \pm h) = \frac{CQE\alpha}{4\pi K(1-\nu)} \left(1 - \frac{2a^2}{b^2 - a^2} \log \frac{b}{a} \right) \quad . \tag{10}$$

Here, $C > 1$ is a factor representing the ratio of $\sigma_\theta(b)$ at the end of the cylinder to its value far from the ends. This factor is not at all well known, and is probably a function of b/a. For a thin-walled cylinder it has been estimated by Kent* to be about 1.3. Provided ν may be regarded as essentially constant for the materials of interest, we may define a material factor, M, as before (Equation 8), and write $Q_{max} = MS$, where the shape factor is now:

$$S = \frac{4\pi(1-\nu)}{C}\left(1 - \frac{2a^2}{b^2-a^2}\log\frac{b}{a}\right) . \qquad (11)$$

The foregoing considerations provide information concerning the shape factor, $S\left(\frac{h}{b}, \frac{b}{a},\right)$ for the hollow cylinder. They suggest that for given b/a it is largest for $\frac{h}{b} = 0$, and then falls off with growing $\frac{h}{b}$, approaching a limit of perhaps 60% of its initial value as $\frac{h}{b}$ becomes large. Experimental results given later indicate the same behavior.

In Appendix A, the first correction to the usual thin-disk equations is discussed. This work has not been carried to a solid conclusion, but it leads us to expect that the shape factor at first decreases in a quadratic manner with $\frac{h}{b}$, as this quantity increases from zero. The expression obtained for the circumferential stress at $r = b$ and $Z = \pm h$ is:

$$\sigma_\theta = \frac{QE\alpha}{4\pi K}\left\{\left(1 - \frac{2a^2}{b^2-a^2}\log\frac{b}{a}\right) + \frac{2(1+\nu)}{3}\frac{h^2}{b^2}\right\} . \qquad (12)$$

---

* C. H. Kent, "Thermal Stresses in Thin-Walled Cylinders", Trans. Am. Soc. Mech. Engr., Vol. 53, pp. 167-180, 1931.

This is almost certainly the maximum tensile stress, which would imply that the shape factor is:

$$S = 4\pi \Big/ \left[1 - \frac{2a^2}{b^2 - a^2} \log \frac{b}{a} + \frac{2(1+\nu)h^2}{3b^2} \right] . \qquad (13)$$

For $b/a = 1.5$, and $\nu = 0.2$, the shape factor for a short cylinder having $\frac{h}{b} = 0.1$ is 2.3% less than that for the indefinitely thin washer.

EXPERIMENTAL TECHNIQUE

Experiments were performed in the thermal-rupture apparatus shown in Figure 1. A detailed description of this equipment and the operating technique is given in Appendix C.

Briefly, the apparatus consists of a graphite resistor rod in an evacuated chamber. The copper walls of the chamber are water cooled, and windows are provided for viewing the specimen during test.

The specimen is a tube which is aligned concentrically on the heater rod at midspan between upper and lower guard tubes. Upon applying power to the rod, heat flows radially through the specimen, producing a temperature drop and resultant thermal stresses. These stresses are increased by increasing the power incrementally until fracture occurs. The power per unit length dissipated through the section of rod opposite the specimen at fracture is recorded. Also, the outer-wall temperature of the specimen is measured with an optical pyrometer, and is recorded at fracture.

In the interests of having steady-state conditions, the increments of power advance are small, and sufficient time is permitted between

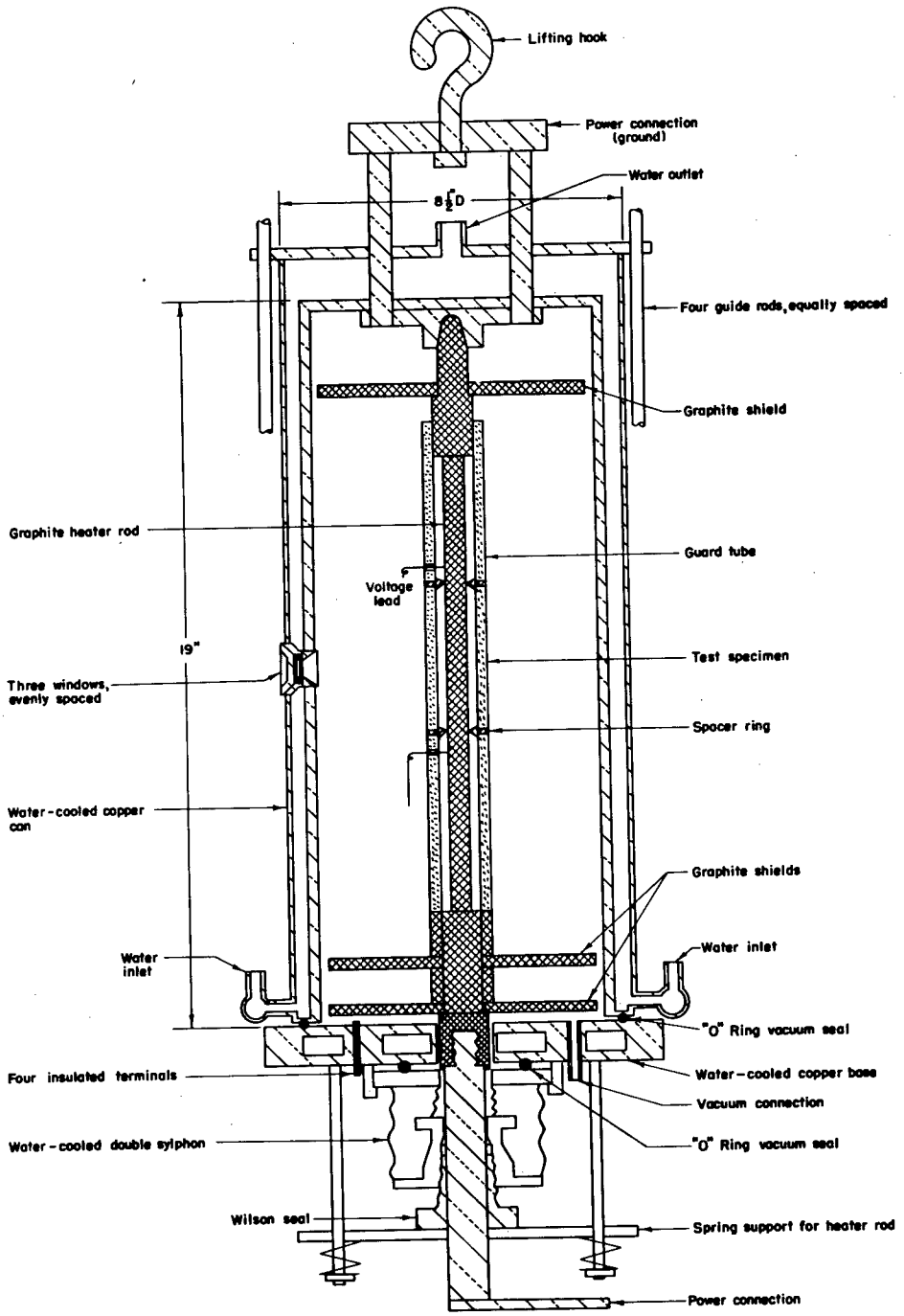

FIGURE 1. SCHEMATIC DIAGRAM OF THERMAL-RUPTURE APPARATUS

power advances for the outer-wall temperature to become constant. Several measures are taken to minimize axial heat flow in the system. Some experimental work in this connection is described in Appendix C.

SPECIMENS

The thermal-rupture data used in this study were from experiments with specimens of either a sintered ruby or a sintered beryllia. The ruby specimens were prepared especially for this study, while the data on the beryllia body were obtained primarily in connection with other work at Battelle on evaluating beryllia bodies.

Sintered Ruby

The inorganic constituents of the raw batch were:

Material	Supplier	Amount, Per Cent
No. 38900 Alundum grain (fused alpha alumina)	Norton Company	95
Chromium sesquioxide (Cr_2O_3) powder, Baker's analyzed	J. P. Baker Chemical Company	5

The batch was supplemented with the following organic additions for plasticizing and green-bonding purposes:

Material	Supplier	Amount Added, Per Cent
Mogul gum, minus 150 mesh (a gelantinized corn starch)	Corn Products Sales Company	3
Gum Ghatti	Innis, Speiden & Company	1

Fifteen per cent of distilled water was added for tempering the batch.

Batches contained 14,000 grams of the inorganic constituents. First, the alumina, chromia, and Mogul gum powders were mixed dry in a water-cooled, 2-1/2-gallon Day mixer, using flat, masticating blades. The gum Ghatti was mixed with 75 per cent of the water in a Waring blendor, and added in this form to the dry-mixed material. The remaining 25 per cent of water also was added at this point, and mixing was continued in the Day mixer for an additional 1-3/4 hours.

The tubular specimens for these studies were formed with a piston-type extrusion apparatus. Details of the forming were the same as given in BMI-T-13* for beryllia bodies.

After extrusion, the tubes were dried in the normal atmosphere of the laboratory for 48 hours, followed by drying at 110 F for 48 hours, and, finally, drying at 180 F for 48 hours.

The extruded stock was next cut with an abrasive wheel into lengths suitable for specimens.

The specimens, enclosed in a muffle of alumina plates, were sintered in a gas-fired furnace. Each specimen was set vertically on a short length of the same extruded stock as used for the specimen. Another short length of tube was placed atop each specimen.

The temperature of the setting was raised to 3100 F in about 24 hours, and held at this temperature for 3 hours. Cooling was then accomplished in the furnace, and required about 20 hours. The total linear shrinkage (drying and sintering) was 12 per cent.

---

* H. Z. Schofield, W. H. Duckworth, R. E. Long, "Fabrication of Beryllia Shapes by Ceramic Extrusion", BMI-T-13, May 1, 1949.

The sintered-ruby specimens had a bulk density of 3.61 g per cu cm. This corresponds to a total porosity of about 9.75 per cent.* The apparent porosity (open pores) was 7.9 per cent.

Sintered Beryllia

The beryllia specimens were formed by plastic extrusion from Refractory-grade beryllia, minus 325 mesh as received, in accordance with the detailed procedure given in BMI-T-13.**

The bulk density of these sintered specimens was 2.15 g per cu cm, corresponding to a total porosity of 29 per cent.

EXPERIMENTAL RESULTS

Effect of Length

Interest exists in the possibility of using the simple product relation, $Q_{max} = MS$, for assessing the resistance of a material, or of a shape to thermal rupture. A thermal-rupture test yields data on Q_{max} only. The influence of either the material properties, expressed by M, or the shape properties, expressed by S, must be determined by other means before the two can be separated. Problems in experimental measurements and treatment of experimental data result in serious objections to the use of physical properties for the direct calculation of M. However, there appears a likely possibility of calculating a suitable S for use as a standard. Also, it is quite significant that the calculated S would be

---

* On the basis of the specific gravity of alpha alumina, taken as 4.0 g per cu cm.

** Ibid.

fairly amenable to experimental checks, while such checks could hardly be used on any values of M determined independently.

Earlier, in the section of this report on theory, three expressions were given for the shape factor, S, of a hollow, circular cylinder under conditions of radial, steady-state heat flow from an external source, as follows:

1. For a very short cylinder:

$$S = 4\pi \Big/ \left(1 - \frac{2a^2}{b^2 - a^2} \ln \frac{b}{a}\right) = \psi \quad . \tag{9}$$

2. For a very short cylinder with a first correction for a length effect:

$$S_1 = \psi \Big/ \left(1 + \frac{(1+\nu)\, h^2 \psi}{6\pi b^2}\right) \quad . \tag{13}$$

3. For a very long cylinder:

$$S_2 = \psi\,(1-\nu)/C \quad . \tag{11}$$

where: a = inner radius,

b = outer radius,

$2h$ = length,

ν = Poisson's ratio,

and C = a constant representing the ratio of tangential stress in the outer wall at the end of a long cylinder to its value far from the end.

From these expressions and the previous theoretical treatment, S is known to decrease when h/b is increased until the limiting case of Equation (11) is approached. Except in the case of Equation (13), little can be deduced about the nature of the relation between S and h/b.

Unfortunately, Equation (13) is only a first correction to the usual thin-disk equation, applicable only when h/b is below the range of practical significance, of the order of 0.1 or less. On the other hand, it is not known how large h/b must be before one can safely use Equation (11), which applies only to an infinitely long tube.

Experimental data were obtained which confirmed and extended these theoretical considerations. They gave evidence of the nature of the relation between S and h/b between the limits of applicability of Equations (13) and (11).

In these experiments, three series of sintered-ruby tubes were fractured in the thermal-rupture apparatus. The tubes in each series had circular cross sections, nominally, 7/8-in. ID and 1-15/16-in. OD, and ranging in length from 1/2 to 6 in. The three series differed only in being fabricated from different raw batches, or sintered at different times. Uncontrolled variables in these fabrication processes introduced slight differences in the internal structure of the tubes, as evidenced by slight differences in the average diameters of the different series.

Average results from the tests are given in Table 1. Each average is based on at least 3, and usually 5 or 6, individual values. The values for Q_{max} and $T_{b\,max}$ from this table are plotted against h/b in Figure 2. It should be pointed out that more care was taken to insure steady-state conditions in Series C than in Series A or B. This fact might account for the lower values of $T_{b\,max}$ in Series A and B.

Figure 2 shows that $T_{b\,max}$, as well as Q_{max}, decreases as h/b is increased. Q_{max} was theorized to decrease, of course, because S in the relation, $Q_{max} = MS$, decreases. The decrease in $T_{b\,max}$ may be explained

TABLE 1. DATA ON LENGTH EFFECTS FOR SINTERED-RUBY TUBES OF THE SAME CROSS SECTION

Series	Tube Dimensions: Length (2ℓ), in.	Tube Dimensions: Average Outer Diameter ($2b$), in.	Tube Dimensions: Average Inner Diameter ($2a$), in.	Shape Parameters: b/a	Shape Parameters: ℓ/b	Average Power Per Unit Length at Fracture, (Q_{max}), watts/cm	Average Outer-Wall Temperature at Fracture ($T_{b\,max}$)*, F
A	4.0	1.315	0.875	1.50	3.04	57	1570
A	2.0	1.312	0.874	1.50	1.52	58	1550
A	1.0	1.312	0.873	1.50	0.76	66	1625
B	4.0	1.339	0.882	1.52	2.99	55	1590
B	2.0	1.335	0.879	1.52	1.50	61	1520
B	1.0	1.342	0.885	1.52	0.75	77	1555
B	0.5	1.339	0.882	1.52	0.37	71	1570
C	6.0	1.320	0.874	1.51	4.55	49	1500
C	4.0	1.322	0.878	1.51	3.02	52	1555
C	3.0	1.322	0.878	1.51	2.27	55	1575
C	2.0	1.322	0.881	1.50	1.51	58	1630
C	1.5	1.320	0.874	1.51	1.14	53	1570
C	1.0	1.320	0.878	1.50	0.76	64	1655
C	0.5	1.320	0.876	1.51	0.38	72	1735

* Uncorrected, optical-pyrometer reading.

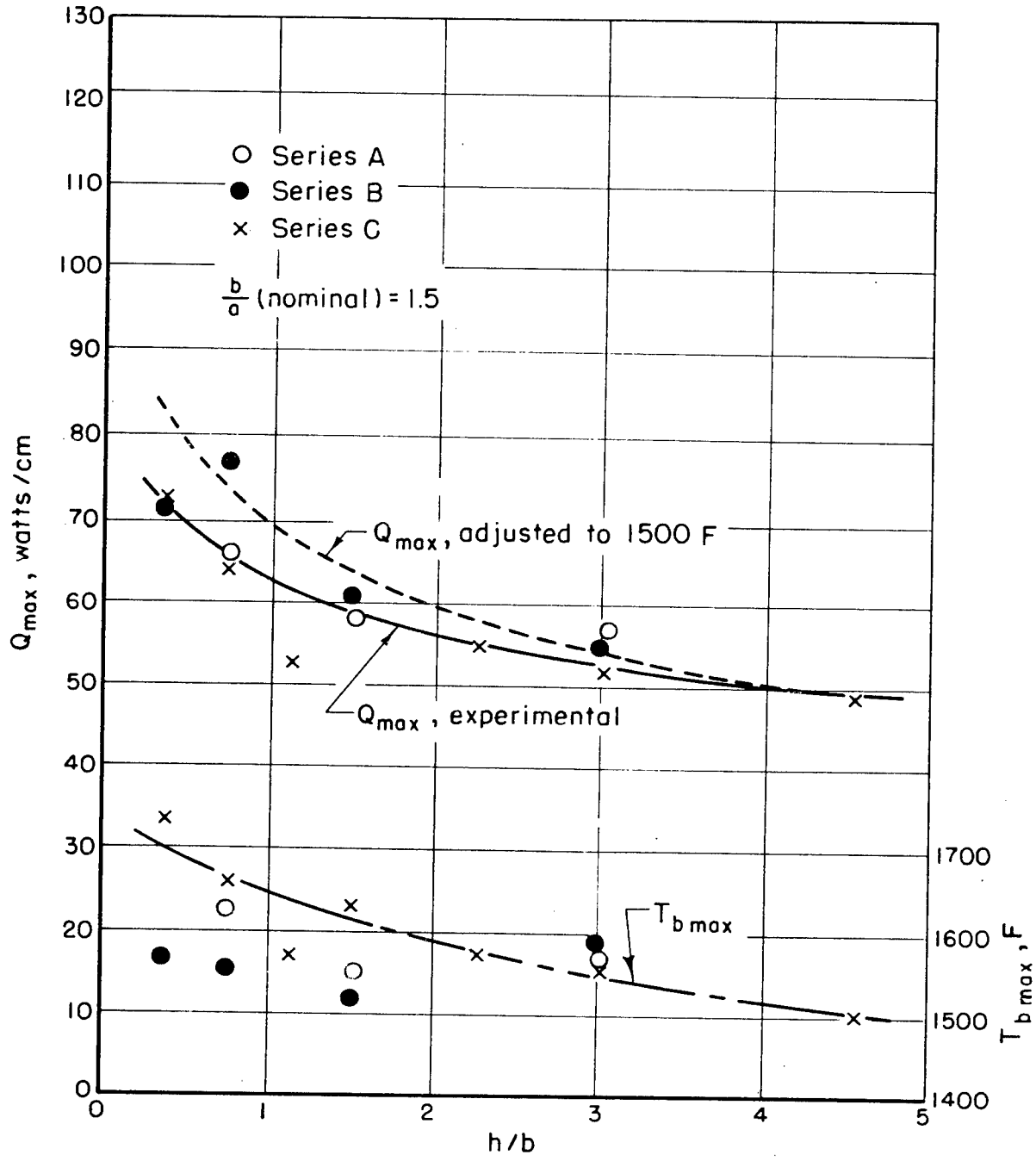

FIGURE 2. VARIATION OF Q_{max} AND $T_{b\,max}$ WITH h/b FOR SINTERED-RUBY TUBES OF THE SAME CROSS SECTION

as follows. The amount of heat which the outer wall radiates to the water-cooled can, which is at an essentially constant temperature, T_c, is proportional to $(T_b^4 - T_c^4)$. Hence, if Q_{max} decreases when h/b is increased, $T_{b\ max}$ also should decrease, as observed.

It is expected that M in the expression, $Q_{max} = MS$, is temperature dependent. Therefore, in view of the variation of $T_{b\ max}$, it is hardly safe to assume that variations in S were solely responsible for the character of the Q_{max} curve. The changes in M with temperature also must be considered. In particular, as the critical tangential stress is at a maximum in the extreme outer fibers, the variation of M with T_b, rather than with the temperature at some other point in the wall, is pertinent here.

As yet, none of the planned experiments have been conducted in the thermal-rupture apparatus on the temperature dependence of M for the sintered ruby. However, data have been obtained, or reported, on the variation with temperature of each of the contributing physical properties, K, P, E, and α. With $M = KP/\alpha E$, where P = a breaking stress, a curve was plotted from these data to approximate the temperature dependence of M. The details of this analysis are covered in a later section of this report, with the resultant curve of M versus temperature shown in Figure 9 (page 43).

Using the approximate variation of M with temperature, so determined, the experimental curve of Q_{max} versus h/b was adjusted to a constant temperature of 1500 F. The resultant curve, representing the variation in S with h/b, is shown along with the experimental curve in Figure 2. A comparison of the two curves indicates that both the

temperature variation of M and changes in S with h/b had appreciable effects on the observed values of Q_{max}. When h/b was decreased from 4.75 to 0.50, S apparently increased about 60 per cent, resulting in an increase in Q_{max} from 49 to 79 watts/cm. However, in the tests, this decrease in h/b caused T_b to increase from 1500 to 1690 F, lowering M and, consequently, Q_{max} from 79 to 70 watts/cm. The net result of the decrease in h/b from 4.75 to 0.50 was an increase of Q_{max} of about 43 per cent, from 49 to 70 watts/cm.

If the adjusted Q_{max} versus h/b curve is extrapolated in both directions, some idea can be obtained of the magnitude of C in Equation (11). When h/b is 0.1, Q_{max} would be about 94. Substituting this value in Equation (13) and assuming $\nu = 0.20$, S_1 for $h/b = 0.1$ is 34.8, and:

$$M = Q_{max}/S_1 = 94/34.8 = 2.7 \text{ watts/cm.}$$

Extrapolating in the other direction, Q_{max} appears to become about 46 watts/cm for very large values of h/b, and:

$$S_2 = \frac{Q_{max}}{M} = \frac{46}{2.7} = 17.0 .$$

Also, from Equation (9), $\psi = 35.6$ when $b/a = 1.5$. Since, for very large values of h/b:

$$C = \frac{\psi(1-\nu)}{S_2}$$

$$= \frac{35.6\ (1-0.20)}{17.0} = 1.68 .$$

This value for C is considerably above the value approximated by Kent,* of about 1.35. Both values, 1.68 and 1.35 are dependent upon the assumed value of ν. Although no determinations have been made on the sintered

---

* Ibid.

ruby, in other work at Battelle, measurements on several different types of ceramic bodies gave values of ν in the range 0.18 - 0.23.

The experimental data are quite meager for general acceptance of the adjusted relation in Figure 2 as that between S and h/b. Confirming data are needed, particularly from thermal-rupture tests on specimens of other materials and with other radii. Also, as indicated, it would be helpful if the value of ν for the sintered ruby were better established. More important, the temperature dependence of ν should be known. Little or no data are available on this relation for ceramic bodies. It was assumed here that ν does not change with temperature. If it does at a significant rate, S . as here defined, ceases to be a valid shape factor and a re-examination of the whole description will be necessary. Thermal-rupture tests on the same shape with variations in the material and in the heat transfer might resolve the problem.

Effect of Radius Ratio

The effect of radius ratio, b/a, on the shape factor, S, is not known for the case of a circular tube of intermediate length subjected to radial, steady-state heat flow from an external source. However, it is reasonable to expect that it will be similar to that for the very short cylinder. Accordingly, experimental results on the effect will be compared with Equation (9), which makes S proportional to ψ . With this proportionality, S would vary with b/a, as shown in Figure 3.

The thermal-rupture data at hand showing the effect of b/a on Q_{max} were obtained on the beryllia body. As pointed out previously, these tests were made in another study at Battelle, where a comparison of

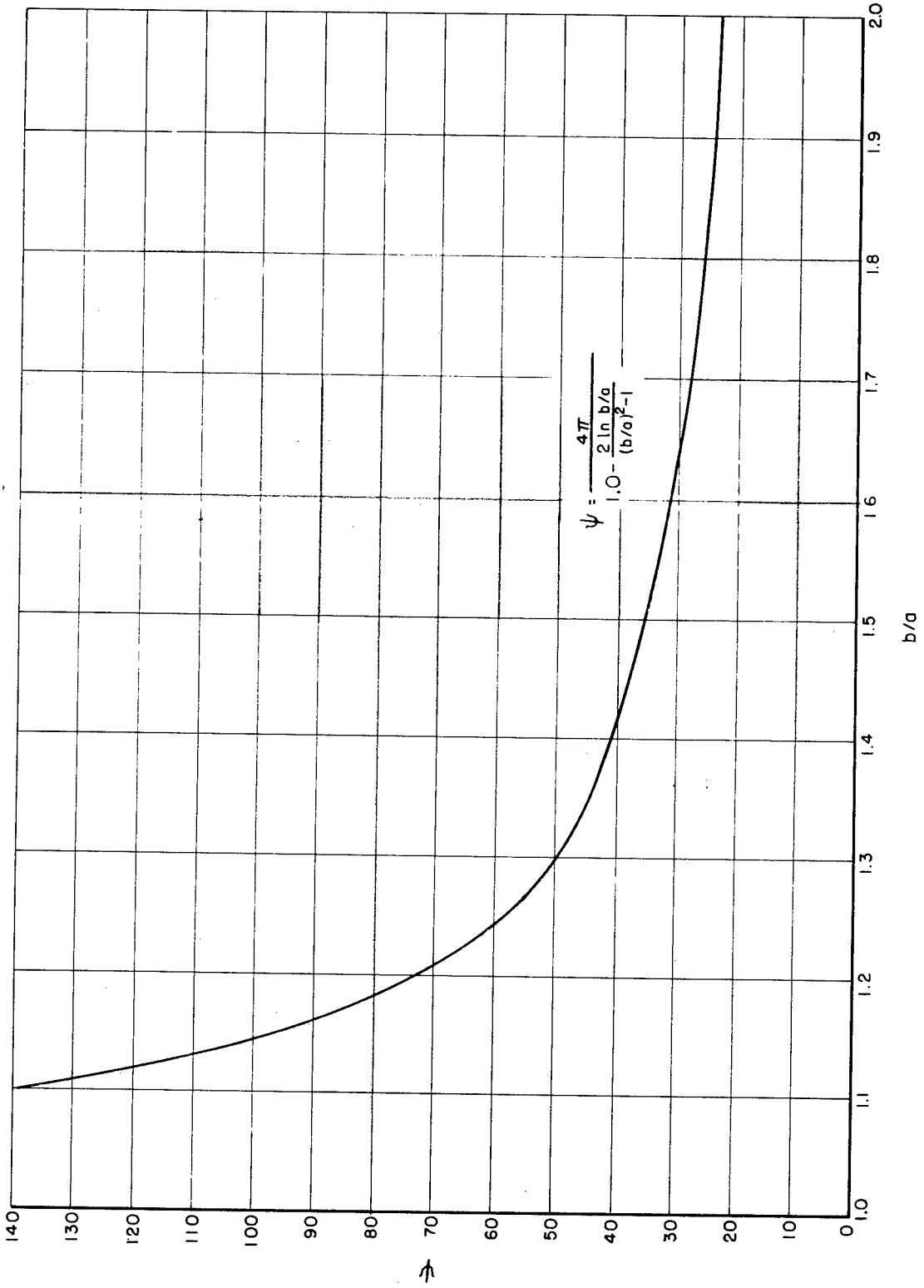

FIGURE 3. THEORETICAL VARIATION OF SHAPE FACTOR WITH b/a FOR A VERY SHORT CYLINDER

the resistances of various beryllia-body developments was of primary interest. Also, the tests were made prior to the present study of thermal rupture and were not run so carefully as those made in connection with the current work. For example, less attention was given to insuring steady-state heat flow, and to uniformity among specimens. As the result of these considerations, some liberty was taken in omitting questionable individual values from the recorded results.

The guard tubes and spacer rings used in these tests were made of the beryllia body, using design "A" in Figure 10 (Appendix C) for the spacer rings. All specimens were 4.0 inches in length (2h). Table 2 gives the results.

In addition to the data in Table 2, several tests were conducted on tubes 1-in. ID and 1-3/8- or 1-1/4-in. OD. The shape parameters were as follows:

OD, in.	b/a	h/b
1-3/8	1.375	2.90
1-1/4	1.250	3.20

All of these thin-walled tubes withstood the maximum safe limit of the thermal-rupture apparatus, corresponding to a Q_{max} of about 320 and 250 watts/cm, respectively, for the 1-3/8- and 1-1/4-inch-OD tubes. The outer wall reached approximately 2600 F for both sizes.

Consider the values of h/b in Table 2, 2.46 and 2.70, when the average Q_{max} was 92 and 106 watts/cm, respectively. On the basis that the adjusted Q_{max} curve in Figure 2 represents the effect of h/b on S, the values of S corresponding to 2.46 and 2.70 are 57.0 and 55.5, respectively. Therefore, to eliminate the influence of h/b from the

TABLE 2. RESULTS OF THERMAL-RUPTURE TESTS ON SINTERED-BERYLLIA TUBES OF TWO SIZES

Test Number	Dimensions: Outer Diameter ($2b$), in.	Dimensions: Inner Diameter ($2a$), in.	Shape Parameters: b/a	Shape Parameters: h/b*	Power Per Unit Length at Fracture (Q_{max}), watts/cm	Outer-Wall Temperature at Fracture** (T_{bmax}), F
52	1.476	0.984	1.50	2.71	110	1675
59	1.483	1.000	1.48	2.70	99	1630
74	1.490	0.987	1.51	2.69	108	1605
78	1.493	0.988	1.51	2.68	106	1605
Average			1.50	2.70	106	1630
114	1.629	1.004	1.62	2.46	94	1440
116	1.623	1.000	1.62	2.46	93	1420
117	1.632	0.999	1.63	2.45	89	1430
Average			1.62	2.46	92	1430

* All tubes were 4.0 inches long ($2h$).

** Uncorrected, optical-pyrometer reading.

data, a corrected Q_{max} of 106 x 57.0/55.5 = 109 watts/cm can be used. This implies that the specimen which failed at 106 watts/cm would have failed at 109 watts/cm if its h/b had been 2.46 instead of 2.70.

The effect of temperature on M must also be considered in determining the effect of b/a on S from these data. As in the case of the ruby body, no thermal-rupture data exist on the temperature dependence of M for the beryllia body. Again, this dependence was estimated from the effect of temperature on the contributing physical properties. Details of the analysis are covered in a later section, with the resultant curve shown in Figure 9 (page 43).

From this curve, M decreases in the ratio 1.05 to 1.00, when T_b is increased from 1430 to 1630 F. Therefore, if the specimens in Table 2 which failed at 106 watts/cm had failed at 1430 F rather than 1630 F, Q_{max} would have been changed further, to 109 x 1.05 = 114 watts/cm.

With this adjustment, a comparison might be made with the theoretical curve in Figure 3. Remember that the use of this curve assumes that b/a enters the expression for S in the same manner for all values of h/b. According to Figure 3, S, hence, Q_{max}, would increase when b/a is decreased from 1.62 to 1.50, in the ratio, 35.6 to 30.5 = 1.17. The experimental data, as adjusted, show that this increase in b/a caused Q_{max} to increase in the ratio, 114 to 92 = 1.24.

The agreement here is fairly good, indicating that S is approximately proportional to Ψ for intermediate lengths. But the experimental evidence is even more limited in scope and extent than that for the effect of length. Also, the discussion of possible sources of error in the

treatment of length effects is equally applicable to this work. Knowledge of the temperature dependence of M and of ν needs to be increased.

The question now arises as to whether the ability of the thin-walled tubes (b/a of 1.375 or 1.25) to withstand the maximum heat flow of the apparatus was normal behavior. From Figure 3, these decreases in b/a should increase S, hence, Q_{max}, above that for the tubes with b/a = 1.50 by the following ratios:

b/a	Ratios of Increase in Q_{max}
1.375	42.5/35.6 = 1.16
1.250	58.0/35.6 = 1.63

As Q_{max} for the tubes with b/a = 1.50 was 106 watts/cm, neglecting temperature and h/b effects, the change in S theoretically would cause Q_{max} for the thin-walled tubes to be:

b/a	Q_{max}, watts/cm
1.375	106 x 1.16 = 123
1.250	106 x 1.63 = 173

Owing to the increase in Q_{max}, $T_{b_{max}}$ also would be higher for the thin-walled tubes than for those with b/a = 1.50. However, as shown in Figure 9, page 43, M decreases as the temperature is increased. For this reason, the tubes would be expected to fracture at values of Q_{max} below 123 or 173 watts/cm. Similarly, as h/b is slightly greater for the thin-walled tubes than for those with b/a = 1.50, S would be less, and Q_{max} would be expected to be lower yet. The fact that they did not fail in the thermal-rupture apparatus at levels above 250 watts/cm, therefore, is particularly interesting.

The possibility that longitudinal planes of weakness were introduced in extruding the thick-walled tubes, and not the thin-walled tubes, was ruled out. Thick-walled tubes ($b/a = 1.5$) which were formed by slip-casting techniques fractured at about the same Q_{max} as those formed by extrusion.

However, an explanation was afforded by considering pyroplastic flow (creep). In rather crude mechanical-loading tests, there was a temperature at which such flow became noticeable in the beryllia body, depending on the load and the time of heating. If these critical conditions were reached in a thermal-rupture test, the thermal stresses undoubtedly would relax, and the specimen would not fail. From this, it appears that fracture can only occur from thermal stresses if the stress required for such fracture is reached before the critical conditions for pyroplastic flow.

The existence of pyroplastic flow in these thin-walled tubes was confirmed in a simple experiment using transient heating. For a given radial heat flow (Q), it is known that the tangential stress in the outer fibers, which causes fracture, builds up during transient heating to a maximum when the heat flow becomes steady state. Since the critical pyroplastic flow is a direct function of stress, time, and temperature, the tubes might fracture at a Q_{max} under transient conditions, with time and temperature suppressed, which they apparently withstand under slowly attained steady-state conditions which permit flow. Such was the case. For example, a tube with a radius ratio (b/a) of 1.375 fractured in about 2 minutes when subjected suddenly to 180 watts/cm. As pointed out before, such tubes withstood 250 watts/cm in the much slower steady-state

test. The stress in the fast test was less than that corresponding to 180 watts/cm in the steady-state test. Further, as the outer-wall temperature at fracture was below 2000 F in the fast test, the strength of the beryllia was lower than at the higher temperature* which was reached at 180 watts/cm in the steady-state test.

Incidentally, as the strength of ceramic bodies increases with increases in the rate of loading, the specimens would be expected to break at an even higher Q_{max} under transient than steady-state conditions, at the same temperature.

From this consideration of pyroplastic flow, the anomalous data from the thin-walled tubes do not vitiate the indication from the thick-walled tubes that S is proportional to Ψ for tubes of intermediate length. Further, it appears that the thermal-rupture apparatus might be used in quantitative studies of pyroplastic flow. The condition with a radius ratio slightly below 1.5 apparently would be the lower limit for critical flow in these particular tests.

TEMPERATURE DEPENDENCE OF MATERIAL FACTOR

Both the experimental analyses of the effect of length and of radius on the shape factor, S, used approximations of the temperature dependence of the material factor, M. The manner of making these approximations is discussed in this section.

As pointed out earlier, thermal-rupture tests have not been conducted, as yet, on either the ruby or beryllia body, to determine the

* Above 2200 F.

variation of M with T_b. Such tests are planned, using a constant shape or a known shape factor, S, and varying the heat transfer in the system. The variation in the heat transfer would, of course, yield different values of $T_{b\,max}$, and corresponding changes in Q_{max}. Then, from the relation, $Q_{max} = MS$, the variation of M with $T_{b\,max}$ could be established.

In lieu of these data, the temperature dependence of M was approximated from the temperature dependence of the individual contributing properties, the relation being:

$$M = \frac{KP}{E\alpha} ,$$

where: K = coefficient of thermal conductivity,

P = critical stress (strength),

α = coefficient of thermal expansion,

E = Young's modulus.

Only the temperature dependence of K, α, and E for the ruby body were determined in connection with this study. These data are plotted in Figure 4. Extruded solid rods were used as specimens. An apparatus of the type described in Research Paper 668, published in 1944 by the National Bureau of Standards, was used for measuring K. A fused-quartz expansion apparatus was used to measure α. This apparatus is described in the National Bureau of Standard's Research Paper 29, 1928. A dynamic (sonic) testing technique was employed for determinations of E*.

Strength-temperature curves for alumina and beryllia were plotted from data published by California Institute of Technology. These curves,

---

* A good description of this method for measuring t is given in C. W. Andrews, "Effect of Temperature on the Modulus of Elasticity", Metal Progress, July, 1950.

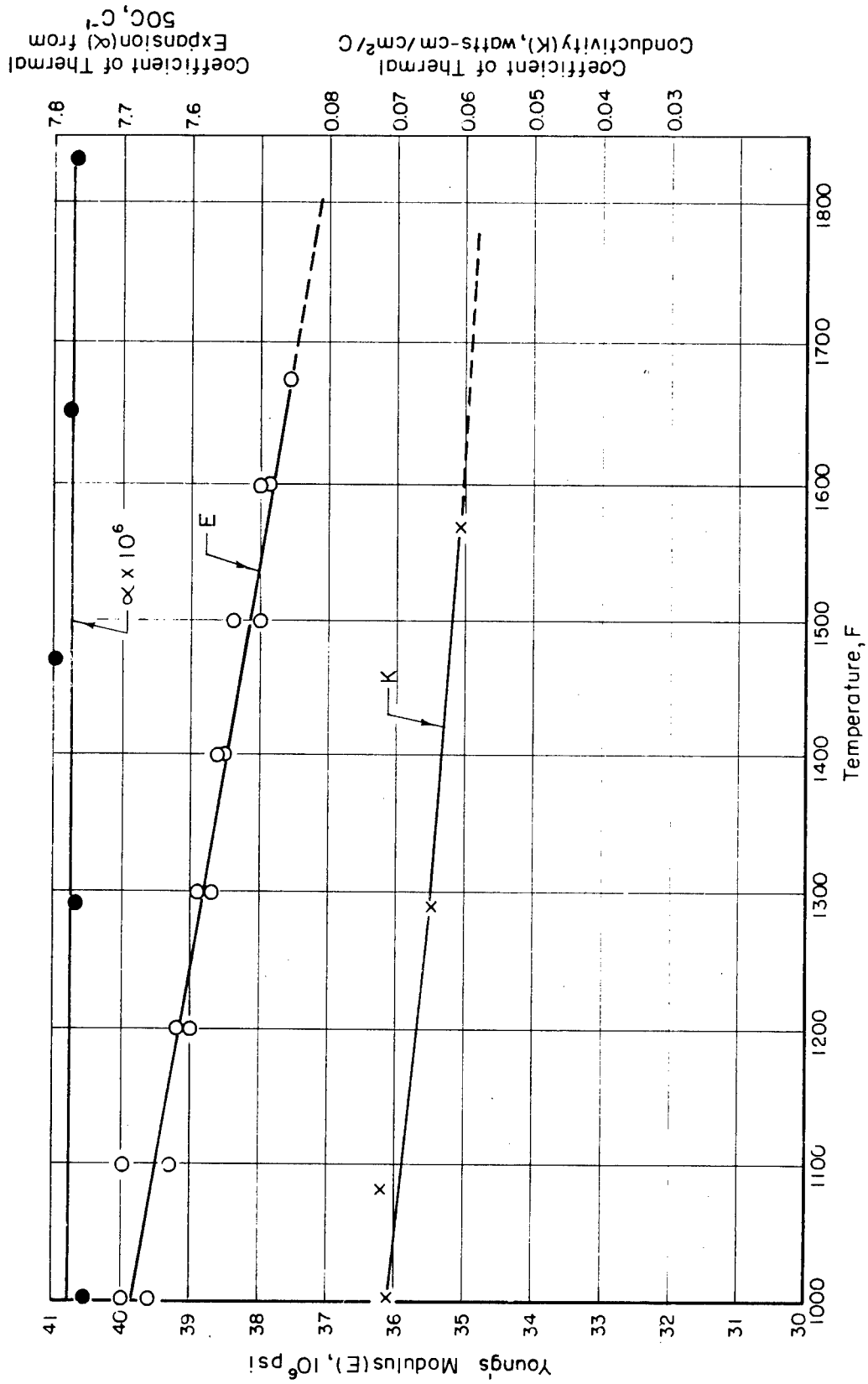

FIGURE 4. TEMPERATURE DEPENDENCE OF PERTINENT PHYSICAL PROPERTIES OF SINTERED RUBY

along with the literature reference, are given in Figures 5 and 6, respectively. The use of the curves involved certain assumptions. In particular, it was assumed that the strength-temperature characteristic was the same for the sintered ruby as for sintered alpha alumina. The fact that ruby is alpha alumina with a small amount of chromia in solid solution gives some basis for this assumption. Also, it was assumed that strength varies with temperature in the same manner for the particular bodies used in this work as for those tested at California Institute of Technology. The fact that Figure 6 shows the same strength-temperature characteristic for two different beryllia bodies supports this assumption. Finally, it was assumed that the critical stress for fracture, P, varies with temperature in the same manner as R, the modulus of rupture in bending, determined by California Institute of Technology. As both the critical thermal stress and the critical bending stress are tensile, this assumption is supported. Further, tests at Ohio State University in bending and direct tension on the same sintered oxide body gave the same strength-temperature characteristic in the elastic region, even though strength values at the same temperature from the two tests were quite different.*

The data on α and K were measured at Battelle on the beryllia body in earlier work for another study. These data were reported in BMI-HRN-11, August 31, 1947. The curves are given in Figure 7. A Young's modulus-temperature curve for sintered beryllia taken from some German

---

* A. P. Welch, "Ceramic Materials for Use in the Design of Jet-Propelled Devices", Report No. 39 from the The Ohio State University Research Foundation to the Air Force, January, 1948.

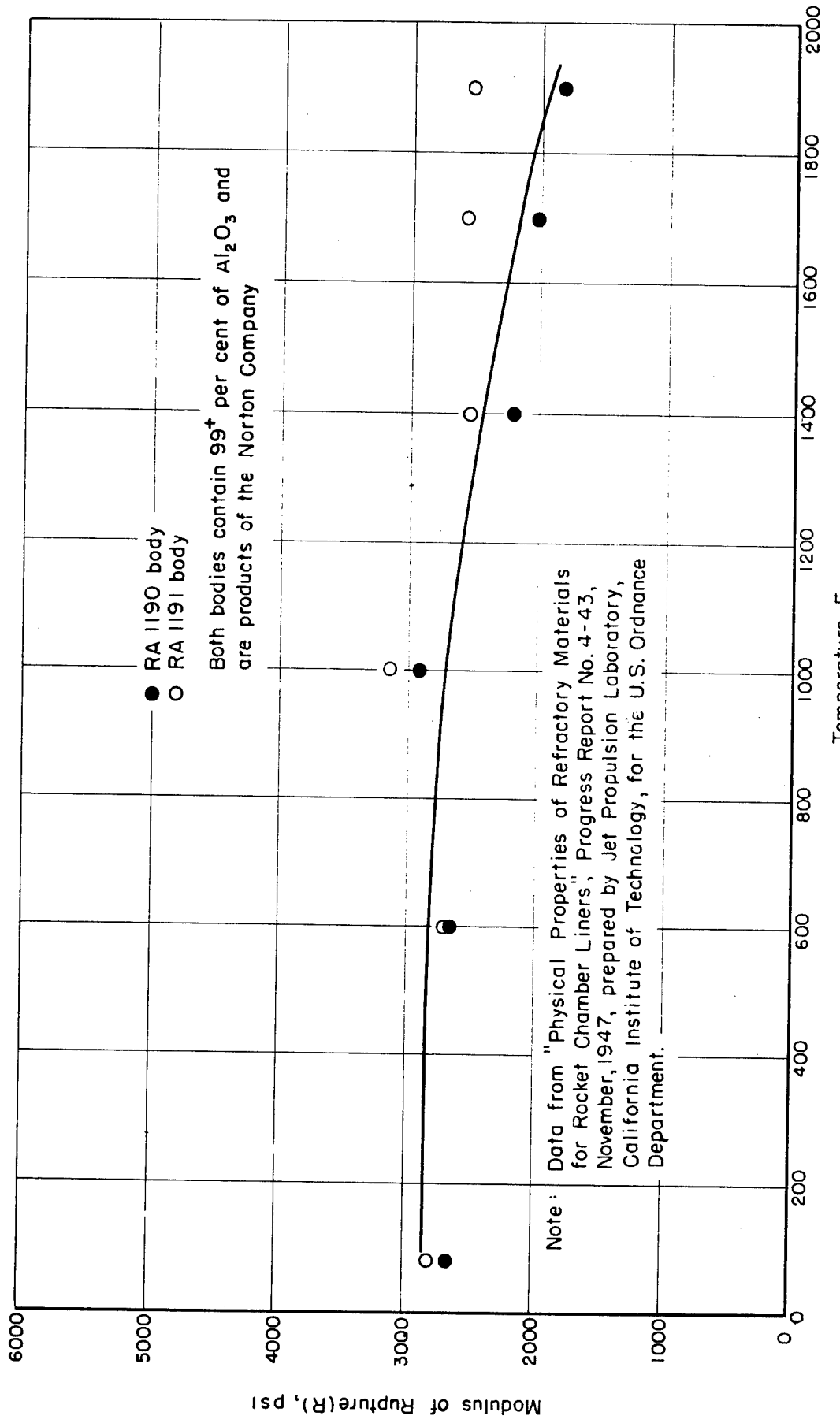

FIGURE 5 EFFECT OF TEMPERATURE ON STRENGTH OF SINTERED ALUMINA

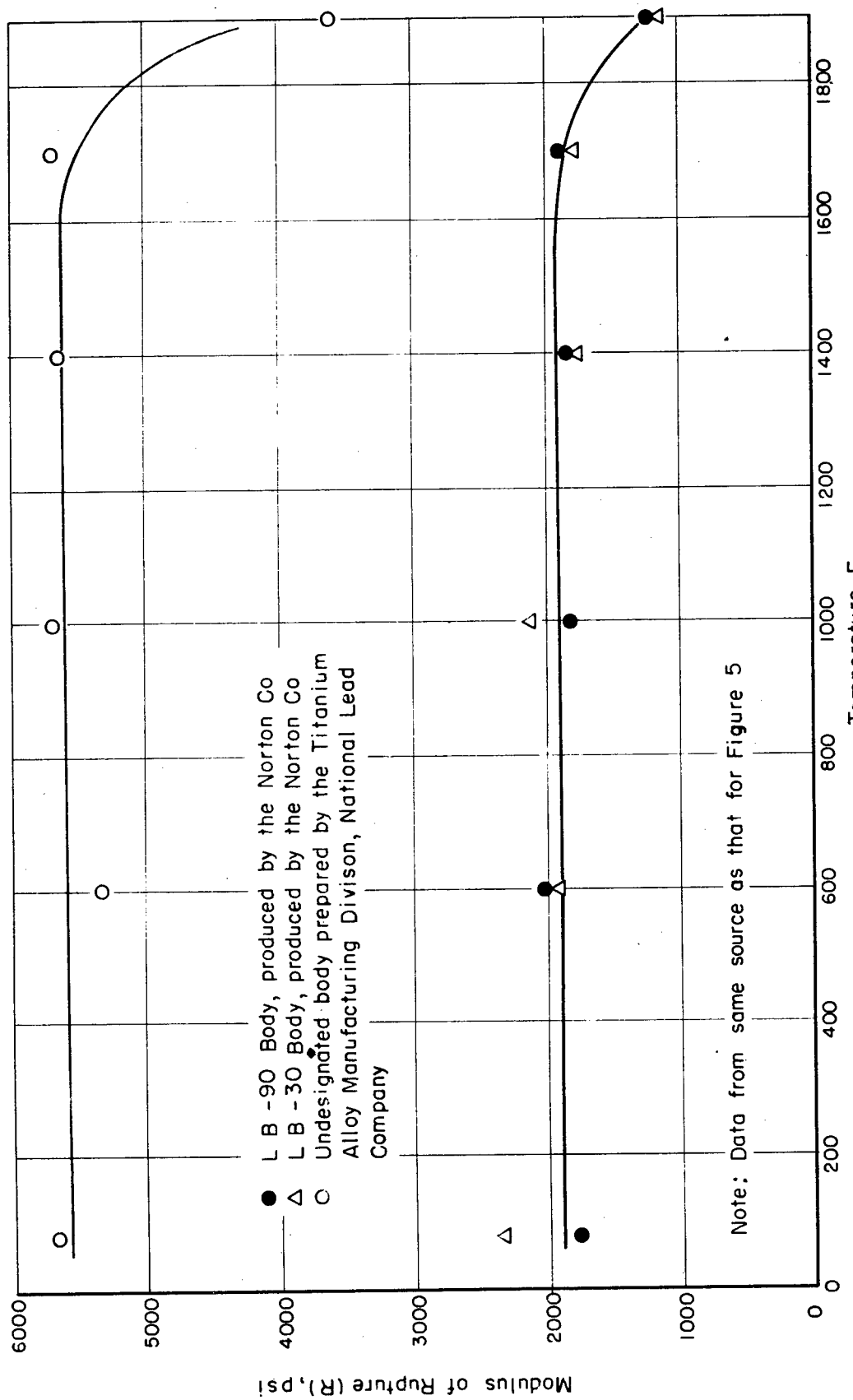

FIGURE 6. EFFECT OF TEMPERATURE ON STRENGTH OF SINTERED BERYLLIA

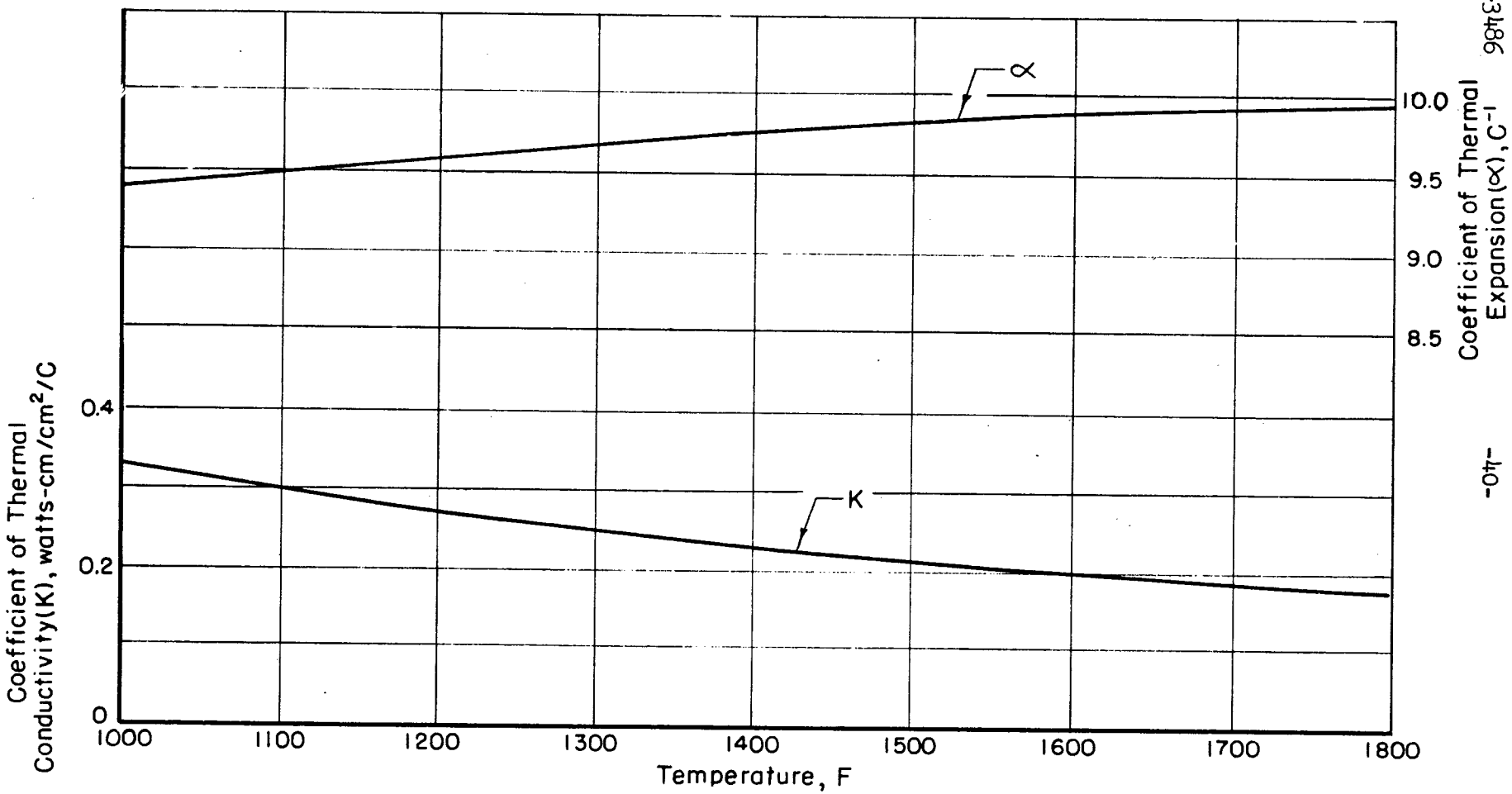

FIGURE 7. THERMAL PROPERTIES OF SINTERED BERYLLIA (FROM BMI-HRN-11, AUGUST 31, 1947)

work was used. The curve and reference are given in Figure 8. It was assumed that E varied with temperature in the same manner for both the sintered beryllia tested in Germany and that used in these studies.

The data on the individual physical properties at various temperatures from Figure 4 through 8 were combined to yield the curves of temperature dependence of M in Figure 9. In view of the assumptions and the combination of any errors in the several tests, the resultant curves cannot be considered very precise.

COMPARATIVE VALUES OF MATERIAL FACTOR FOR THE RUBY AND BERYLLIA BODIES

It might be of interest to compare the resistance to thermal rupture of the ruby and beryllia bodies on the basis of these experimental data. Earlier, with ν assumed to be 0.2 at all temperatures, C was calculated to be 1.68, and M for the ruby body at 1500 F, became 2.7 watts/cm.

With this same assumption concerning ν, M at 1630 F for the beryllia body becomes:

$$M_{(T=1630\,F)} = \frac{Q_{max}}{S(b/a = 1.5,\ h/b = 2.7)} =$$

$$\frac{106}{17.0 \times \frac{55.5}{46}} = 5.16 \text{ watts/cm.}$$

In this calculation, the term 17.0 is the shape factor for a very long tube with $b/a = 1.5$, from Equation (11), while the term 55.5/46 is the adjustment of this shape factor for length, from Figure 2. To get the values of M on the same temperature basis, the adjustment, from Figure 9 is: $M_{(T=1500)} = M_{(T=1630)} \times \frac{1.02}{1.00} = 5.16 \times \frac{1.02}{1.00} = 5.26$ watts/cm.

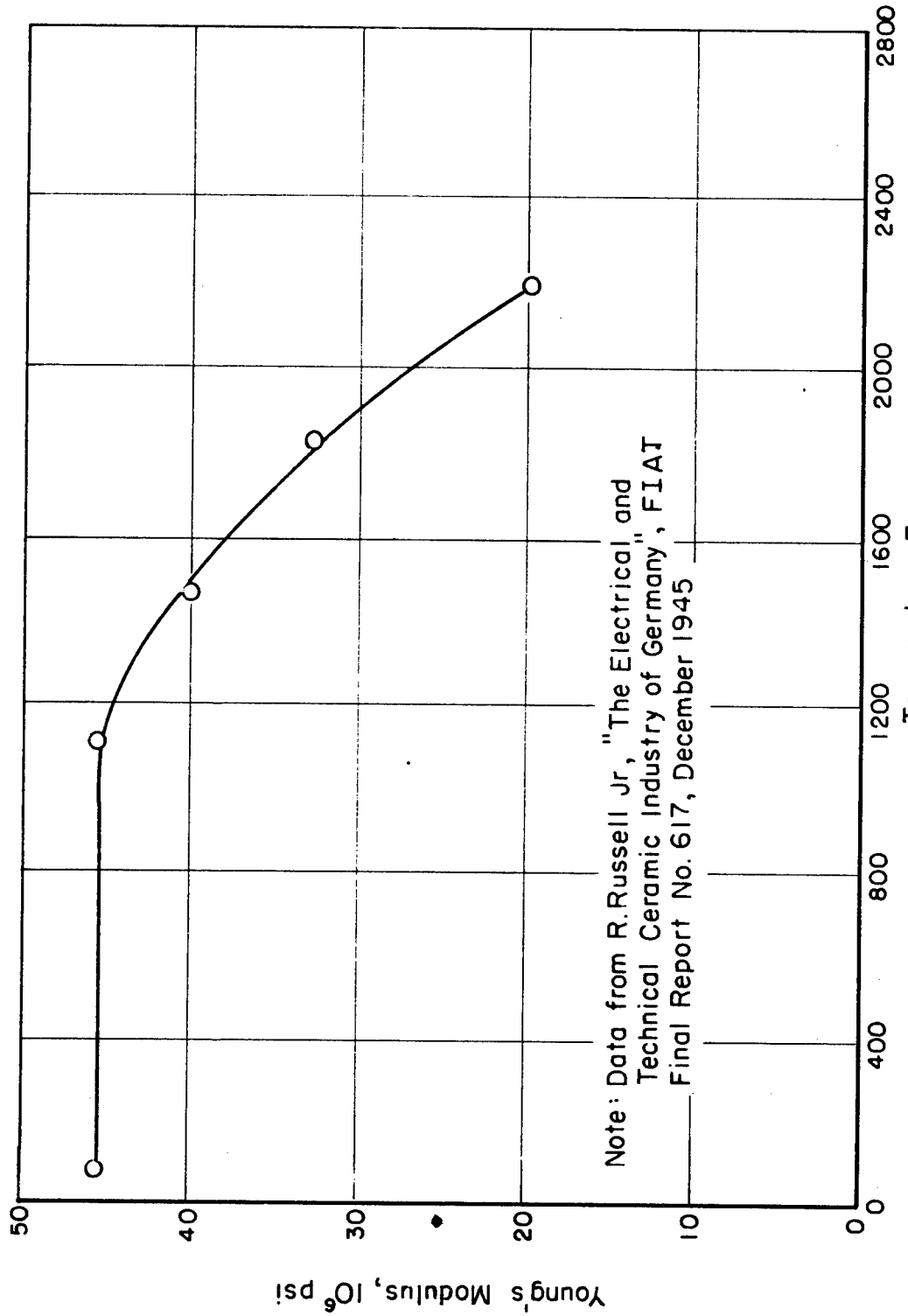

FIGURE 8. EFFECT OF TEMPERATURE ON YOUNG'S MODULUS OF SINTERED BERYLLIA

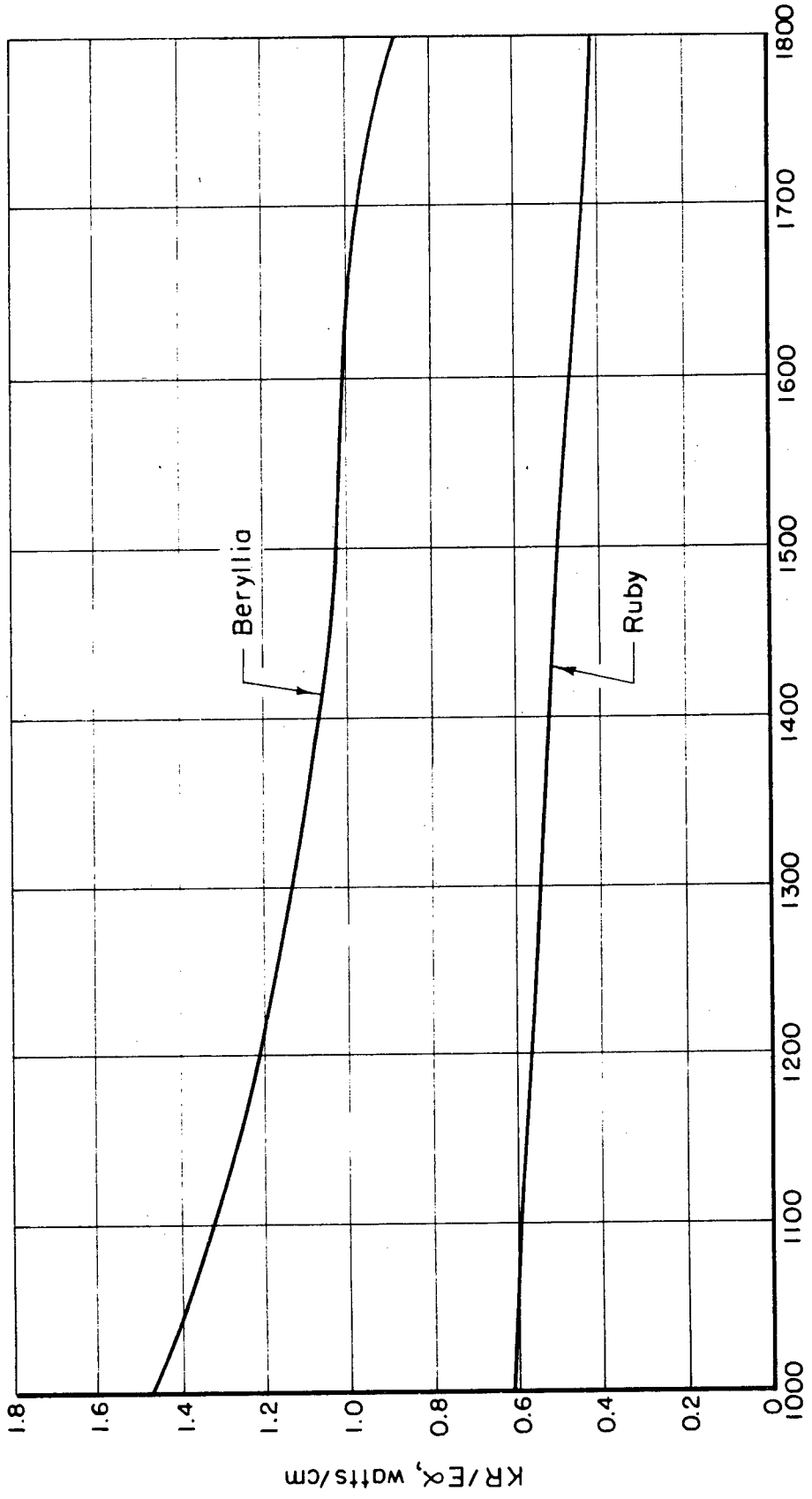

FIGURE 9. ESTIMATED EFFECT OF TEMPERATURE ON THE MATERIAL FACTOR OF SINTERED RUBY AND SINTERED BERYLLIA

From this, if the cooled wall of a fuel element is to be maintained at 1500 F, almost twice as much power could be extracted safely by using the beryllia body rather than the ruby body. If the shape factor for the element were known, the amount of this power could be determined. These findings, of course, might change as the theoretical and experimental work is extended beyond these preliminary stages.

It should be noted that the result of this comparison would be the same if a value for C other than 1.68 had been used. The actual values of M for both bodies would change proportionally with a different C, hence, a different S. In other words, it is important to establish a standard M or S which will define Q_{max}. The matter of proportion between M and S is not important for design or appraisal purposes so long as the basis for arriving at the standard is known, and so long as the effect of all possible variables on M or S is known.

EMB/WHD/EMS/HZS:lkm
May 31, 1951

APPENDIX A

Thermal Stresses in Thin Discs

Consider a disc bounded by the surfaces $z = \pm h, r = a, r = b$, where $h \ll a < b$. It is free from external forces, stresses being brought about by a temperature distribution described by $T(r)$, a function of r only. Calculation of the stresses in first approximation is outlined in a number of places.* Here, an account is given of progress towards a higher approximation which does not entirely neglect the finite value of h/a. In seeking a solution, the conditions to be satisfied are as follows:

(1) Hooke's law relations between stress and strain,

(2) Compatibility equations for the strain components,

(3) The partial differential equations for equilibrium within the body,

(4) Absence of all external forces.

The second of these requirements will be satisfied automatically by adopting expressions for the components of the displacement vector and deducing strain components from them. From the axial symmetry of the problem it is evident that the circumferential component of displacement is zero, and that the radial and axial components, u and w, are functions of r and z only. For these components we may try expansions

---

* For example, S. Timoshenko, "Theory of Elasticity" (McGraw-Hill Book Company, New York, 1934), § 113. Chapter 11 gives a general discussion of axially symmetric stress distributions.

in powers of z. Retaining those terms needed to give an approximation one step beyond the usual one, we have:

$$u = f_1(r) + (h^2 - 3z^2) f_2(r) \quad , \tag{A1}$$

$$w = z g_1(r) + (h^2 z - z^3) g_2(r) \quad . \tag{A2}$$

It is clear from symmetry that the radial displacement must be an even function of z, and the axial, odd. Introduction of h^2 into the second terms of the expressions is a convenience. The strain components corresponding to (A1) and (A2) are:

$$\epsilon_r = \frac{\partial u}{\partial r} = \frac{df_1}{dr} + (h^2 - 3z^2)\frac{df_2}{dr} \quad ,$$

$$\epsilon_\theta = \frac{u}{r} = \frac{f_1}{r} + (h^2 - 3z^2)\frac{f_2}{r} \quad ,$$

$$\epsilon_z = \frac{\partial w}{\partial z} = g_1 + (h^2 - 3z^2) g_2 \quad ,$$

$$\gamma_{rz} = \frac{\partial u}{\partial z} + \frac{\partial w}{\partial r} = z\left(\frac{dg_1}{dr} - 6f_2 + \left[h^2 - z^2\right]\frac{dg_2}{dr}\right) .$$

The term of order h^3 in γ_{rz} actually lies beyond the present approximation and will be dropped from this point on. Stresses may then be obtained by inserting these strains into the Hooke's law equations:

$$\sigma_r = \frac{E}{(1+\nu)(1-2\nu)}\left\{(1-2\nu)\epsilon_r + \nu\Delta - (1+\nu)\alpha T\right\} ,$$

$$\sigma_\theta = \frac{E}{(1+\nu)(1-2\nu)}\left\{(1-2\nu)\epsilon_\theta + \nu\Delta - (1+\nu)\alpha T\right\} ,$$

$$\sigma_z = \frac{E}{(1+\nu)(1-2\nu)}\left\{(1-2\nu)\epsilon_\theta + \nu\Delta - (1+\nu)\alpha T\right\} ,$$

$$\tau_{rz} = \frac{E}{2(1+\nu)}\gamma_{rz} ,$$

where $\Delta = \epsilon_r + \epsilon_\theta + \epsilon_z$ is the dilatation. Thus one obtains:

$$\sigma_r = \frac{E}{(1+\nu)(1-2\nu)}\left\{\left[(1-2\nu)\frac{df_1}{dr} + \nu\Delta_1 - (1+\nu)\alpha T'\right] - (3z^2 - h^2)\left[(1-2\nu)\frac{df_2}{dr} + \nu\Delta_2\right]\right\},$$

$$\sigma_\theta = \frac{E}{(1+\nu)(1-2\nu)}\left\{\left[(1-2\nu)\frac{f_1}{r} + \nu\Delta_1 - (1+\nu)\alpha T'\right] - (3z^2 - h^2)\left[(1-2\nu)\frac{f_2}{r} + \nu\Delta_2\right]\right\},$$

$$\sigma_z = \frac{E}{(1+\nu)(1-2\nu)}\left\{\left[(1-2\nu)g_1 + \nu\Delta_1 - (1+\nu)\alpha T'\right] - (3z^2 - h^2)\left[(1-2\nu)g_2 + \nu\Delta_2\right]\right\},$$

$$\tau_{rz} = \frac{Ez}{2(1+\nu)}\left(\frac{dg_1}{dr} - 6f_2\right),$$

where: $\Delta_1 = \frac{df_1}{dr} + \frac{f_1}{r} + g_1$, and, $\Delta_2 = \frac{df_2}{dr} + \frac{f_2}{r} + g_2$

It is now necessary to choose the functions, f_1 , f_2 , g_1 , and g_2 , so as to satisfy as well as possible the conditions on the stresses. These are the differential equations for equilibrium:

$$r\frac{\partial \sigma_z}{\partial z} + \frac{\partial}{\partial r}(r\tau_{rz}) = 0 \ , \qquad \text{(A3)}$$

$$r\frac{\partial \sigma_r}{\partial r} + (\sigma_r - \sigma_\theta) + r\frac{\partial \tau_{rz}}{\partial z} = 0 \ , \qquad \text{(A4)}$$

and the boundary conditions:

$$\sigma_z = \tau_{rz} = 0 \quad \text{at} \quad z = \pm h \ ,$$

$$\sigma_r = \tau_{rz} = 0 \quad \text{at} \quad r = a \ \text{and} \ r = b \ .$$

The solution to be given below satisfies all of these requirements to the proper approximation, except the vanishing of σ_r at the edges of the disc. This failure leaves an important part of the problem unsolved, but, as will be shown, some tentative conclusions of value can be drawn all the same.

From the vanishing of τ_{rz} on the plane boundaries and the first of the differential equations for equilibrium (A3), it can be concluded that $\frac{\partial \sigma_z}{\partial z}$ is zero on these boundaries. From this condition and that for σ_z itself, it follows that in the present approximation σ_z is everywhere zero, and the unknown functions satisfy the equations:

$$(1-\nu)g_1 + \nu\left(\frac{df_1}{dr} + \frac{f_1}{r}\right) = (1+\nu)\alpha T \,, \tag{A5}$$

$$(1-\nu)g_2 + \nu\left(\frac{df_2}{dr} + \frac{f_2}{r}\right) = 0 \,. \tag{A6}$$

Further, since σ_z is everywhere zero, Equation (A3) indicates that τ_{rz} is a function of z only, divided by r. The boundary conditions at $r = a$ and $r = b$ then require that τ_{rz} be zero everywhere. This gives the equation:

$$f_2 = \frac{1}{6}\left(\frac{dg_1}{dr}\right) \,, \tag{A7}$$

and reduces the radial equilibrium equation to:

$$r\frac{\partial\sigma_r}{\partial r} + \sigma_r - \sigma_\theta = 0 \,. \tag{A8}$$

This is satisfied to lowest order, provided:

$$(1-\nu)\left(\frac{df_1}{dr} + \frac{f_1}{r}\right) + \nu g_1 = (1+\nu)\alpha T + \text{Const.} \tag{A9}$$

It is not necessary to consider the radial equilibrium equation in the next higher order, since this would bring in terms of order z^3 in τ_{rz}, which have been omitted from the beginning.

The First Approximation for σ_r and σ_θ

From Equations (A5) and (A9) one obtains:

$$g_1 = (1+\nu)\alpha T + \nu A \,, \tag{A10}$$

$$\frac{df_1}{dr} + \frac{f_1}{r} = (1+\nu)\alpha T - (1-\nu)A \,, \tag{A11}$$

where A is a constant to be determined by the appropriate boundary condition -- that the contribution to σ_r from f_1 and g_1 should vanish at $r = a$ and $r = b$. These are the correct conditions since the correction terms which follow from the assumed displacements cannot be made to

vanish at the boundaries for all z, but do produce zero resultant force and zero moment when integrated over z. On integrating the equation for f_1, using it along with g_1, and taking account of the boundary conditions, the following contributions to σ_r and σ_θ are obtained:

$$\frac{E\alpha}{r^2}\left\{\frac{r^2-a^2}{b^2-a^2}\int_a^b T r\,dr - \int_a^r T r\,dr\right\}. \tag{A12}$$

$$\frac{E\alpha}{r^2}\left\{\frac{r^2+a^2}{b^2-a^2}\int_a^b T r\,dr + \int_a^r T r\,dr - T r^2\right\}. \tag{A13}$$

These agree with the expressions usually given, and for external heating lead to a circumferential stress at the surface:

$$\sigma_\theta(b) = \frac{Q E \alpha}{4\pi K}\left(1 - \frac{2a^2}{b^2-a^2}\log\frac{b}{a}\right). \tag{A14}$$

where Q is the power per unit length passing outward through the cylinder wall.

Correction Terms

Using Equation (A7) we have:

$$f_2 = \frac{1}{6}\frac{dg_1}{dr} = \frac{\alpha(1+\nu)}{6}\frac{dT}{dr}. \tag{A15}$$

Then, from Equation (A6):

$$g_2 = \frac{-\alpha\nu(1+\nu)}{6(1-\nu)}\left(\frac{d^2T}{dr^2} + \frac{1}{r}\frac{dT}{dr}\right). \tag{A16}$$

For external heating, which is of most interest at the moment, g_2 vanishes. In fact, $\frac{dT}{dr} = \frac{-Q}{2\pi K r}$ and

$$f_2 = \frac{-Q\alpha(1+\nu)}{12\pi K r}. \tag{A17}$$

The complete expressions for the stresses σ_r and σ_θ at $r = b$ then become:

$$\sigma_r(b,z) = -\frac{QE\alpha}{4\pi K}\left(\frac{3z^2-h^2}{3b^2}\right), \tag{A18}$$

$$\sigma_\theta(b,z) = \frac{QE\alpha}{4\pi K}\left\{\left(1-\frac{2a^2}{b^2-a^2}\log\frac{b}{a}\right)+\frac{(3z^2-h^2)}{3b^2}\right\}. \tag{A19}$$

The assumed displacements have not led to a complete solution of the proposed problem. As was anticipated above, the stress $\sigma_r(b,z)$ is zero only for particular values of z. It is true that the resultant force and the resultant moment per unit length of the edge, obtained by suitable integrations over z, do vanish, so that for points away from the edges a higher approximation to the stresses has been obtained. However, it is only the stress at $r = b$ which is of most interest. The calculations should therefore be carried further by examining the effect on σ_θ of applying a radial stress at the boundary which is the reverse of the value given in Equation (A18). This part of the work is not complete, but a tentative result for the maximum tensile stress is reached in the following paragraph. This result is almost certainly correct to the present approximation, that is, to order h^2/b^2.

In view of Saint-Venant's principle, we may expect that added stresses arising from a load,

$$\sigma_r'(b,z) = \frac{QE\alpha}{12\pi K b^2}(3z^2-h^2), \tag{A20}$$

will be localized near $r = b$, and that the curvature of the edge of the disc will play no important role. Thus, the strain component

$$\epsilon_\theta' = \frac{u'}{r} = \frac{1}{E}\left\{\sigma_\theta' - \nu(\sigma_r' + \sigma_z')\right\}. \tag{A21}$$

is likely to be negligibly small, so that σ_θ' may be approximated by:

$$\sigma_\theta' = \nu(\sigma_r' + \sigma_z') \quad . \tag{A22}$$

Further, at the ends of the short cylinder, namely $z = \pm h$, $\sigma_z' = 0$.

Thus:

$$\sigma_\theta'(b, \pm h) = \nu\sigma_r'(b, \pm h) = \frac{\nu Q E \alpha h^2}{6\pi K b^2} \quad . \tag{A23}$$

Adding this to the value given by Equation (A19) we have:

$$\frac{QE\alpha}{4\pi K}\left\{\left(1 - \frac{2a^2}{b^2-a^2}\log\frac{b}{a}\right) + \frac{2(1+\nu)h^2}{3b^2}\right\} \quad . \tag{A24}$$

Although the variation of $\sigma_\theta'(b, z)$ with z has not been considered here, we can be rather sure that the maximum values of the final $\sigma_\theta(b, z)$ do occur at $z = \pm h$, so that Equation (A24) gives the maximum tensile stress. The corresponding shape factor, S, is given by:

$$\frac{4\pi}{S} = \left(1 - \frac{2a^2}{b^2-a^2}\log\frac{b}{a}\right) + \frac{2(1+\nu)h^2}{3b^2} \quad . \tag{A25}$$

APPENDIX B

The Effect of Temperature Dependence of Material Parameters on the Thermal Rupture of Brittle Cylinders

In the calculation of thermal stresses, the temperature dependence of material parameters, such as the thermal conductivity and elastic moduli, is usually neglected. In this appendix the influence of such dependence on the conditions for thermal rupture of a long, hollow cylinder will be considered. Attention will be given to a cylinder entirely free of external load in which heat flows radially from the inner to the outer wall. Only the steady-state problem will be considered.

According to the usual calculation, the maximum value of the tangential, tensile stress, σ_θ, occurs at the outer surface, and, for points far removed from the ends of the cylinder, is given by:

$$\sigma_\theta(b) = \frac{Q E \alpha}{4\pi K(1-\nu)} \left(1 - \frac{2a^2}{b^2-a^2} \log \frac{b}{a} \right), \qquad \text{(B1)}$$

where: Q = power put through per unit length,

α = coefficient of linear expansion,

E = Young's modulus,

ν = Poisson's ratio,

a = inner radius of the cylinder,

b = outer radius.

At points away from the ends of the cylinder, the axial stress at the surface, $\sigma_z(b)$, turns out to be equal to $\sigma_\theta(b)$, as given by Equation (B1). As the ends of the cylinder are approached it is evident that $\sigma_z(l)$ will decrease toward zero, while approximate calculations indicate

that $\sigma_\theta(b)$ increases somewhat. Thus, if the material fails when some critical tensile stress, P, is reached, an axial crack starting near one end of the cylinder is to be expected. Experiments on ceramic bodies are in agreement with this expectation. Thus, end effects are apparently of primary importance in determining how failure occurs. However, since end corrections are moderate, it is still justified to use Equation (B1) as a rough approximation in discussing conditions for failure. On this basis, failure is to be expected when the right side of Equation (B1) reaches the critical stress, P. The corresponding maximum power per unit length is:

$$Q_{max} = \frac{4\pi K P(1-\nu)}{E\alpha} \Big/ \left(1 - \frac{2a^2}{b^2-a^2} \log \frac{b}{a}\right). \qquad (B2)$$

Thus, in this case, Q_{max} is found to be the product of a factor depending on the physical parameters of the material, and a second factor depending on the ratio, b/a; that is on the geometry of the cross section of the cylinder. Here, this type relation for Q_{max} has been reached in a very special way, and it is granted that more general approaches are possible. However, it is clear that such a simple separation of material and shape into distinct factors will not hold rigorously when the problem is generalized. Here, one type of generalization will be examined. The modifications of Equations (B1) and (B2) resulting from <u>small</u> variations with temperature of the physical parameters, K, α, E, and ν, will be sought. This seems particularly desirable in view of interest in the temperature dependence of Q_{max}, and a wish to describe this in terms of a temperature-dependent materials factor, if this is permissible.

The Temperature Distribution

The main task, that of calculating stresses from the temperature distribution, is taken up in the next section. Here, the simpler question of the temperature distribution is considered. The temperature is a function of the radius r only, and is obtained by integrating the differential equation:

$$-2\pi r K \frac{dT}{dr} = Q \quad . \tag{B3}$$

We assume that the conductivity varies linearly with the temperature:

$$K = K_b \left\{ 1 + \lambda (T - T_b) \right\} , \tag{B4}$$

the subscript b referring to conditions at the outer surface of the cylinder. We further assume that $|\lambda(T - T_b)| << 1$ throughout the cylinder, and look for an expression for $T(r)$ which is correct to first order in λ. To this approximation:

$$dT = \frac{-Q}{2\pi K_b} \left\{ 1 - \lambda (T - T_b) \right\} \frac{dr}{r} \quad . \tag{B5}$$

When the λ term is neglected this integrates to:

$$T - T_b = \frac{Q}{2\pi K_b} \log \frac{b}{r} \quad . \tag{B6}$$

Using Equation (B6) in the λ term in Equation (B5) and completing the integration, the desired approximation is obtained:

$$T - T_b = \frac{Q}{2\pi K_b} \left(\log \frac{b}{r} \right) \left\{ 1 - \frac{\lambda Q}{4\pi K_b} \log \frac{b}{r} \right\} \quad . \tag{B7}$$

At a later stage the following average will be wanted:

$$\langle T - T_b \rangle = \frac{2}{b^2 - a^2} \int_a^b (T - T_b) r \, dr \quad . \tag{B8}$$

This is:

$$\langle T - T_b \rangle = \frac{Q}{2\pi K_b} \left\langle \log \frac{b}{r} \right\rangle \left\{ 1 - \frac{\lambda Q}{4\pi K_b} \frac{\left\langle \left(\log \frac{b}{r} \right)^2 \right\rangle}{\left\langle \log \frac{b}{r} \right\rangle} \right\}, \quad \text{(B9)}$$

where:

$$\left\langle \log \frac{b}{r} \right\rangle = \frac{1}{2} - \frac{a^2}{b^2 - a^2} \log \frac{b}{a} . \quad \text{(B10)}$$

$$\left\langle \left(\log \frac{b}{r} \right)^2 \right\rangle = \frac{1}{2} - \frac{a^2}{b^2 - a^2} \left\{ \left(\log \frac{b}{a} \right)^2 + \log \frac{b}{a} \right\} . \quad \text{(B11)}$$

The Calculation of Stress

The appropriate Hooke's law equations, written for cylindrical coordinates, r, θ, z, and giving the stress components, σ_r, σ_θ, σ_z, are:

$$\sigma_r = \frac{E}{1+\nu} \left\{ \epsilon_r + \frac{\nu \Delta}{1-2\nu} - \left(\frac{1+\nu}{1-2\nu} \right) y_0(r) \right\} , \quad \text{(B12)}$$

plus two others obtained by changing the subscripts of σ_r and ϵ_r to θ and z. Here: $\epsilon_r = \frac{\partial u}{\partial r}$, $\epsilon_\theta = \frac{u}{r}$, $\epsilon_z = \frac{\partial w}{\partial z}$ (the strain components for the case of axial symmetry), u and w being radial and axial components of the displacement vector. $\Delta = \epsilon_r + \epsilon_\theta + \epsilon_z = \frac{1}{r} \frac{\partial}{\partial r} (ru) + \epsilon_z$ is the dilatation; and $y_0(r) = \int_{T_b}^{T(r)} \alpha \, dT$. As is usually done in calculations of stresses away from the ends of a long cylinder, $\epsilon_z = \frac{\partial w}{\partial z}$ is to be assumed constant.

In the present problem the shear stresses, $\tau_{r\theta}$, etc. are zero, and body forces are insignificant. The corresponding differential equations for equilibrium are:

$$\frac{\partial \sigma_r}{\partial r} + \frac{\sigma_r - \sigma_\theta}{r} = 0 \qquad \frac{\partial \sigma_\theta}{\partial \theta} = 0 \qquad \frac{\partial \sigma_z}{\partial z} = 0 . \quad \text{(B13)}$$

With ϵ_z constant, the last of these equations establishes that the dilatation, Δ, is a function of r only. The second is automatically covered by the axial symmetry which characterizes the problem. The first will provide a differential equation for the radial displacement, $u(r)$. From Equation (B12):

$$\frac{\partial \sigma_r}{\partial r} = \frac{E}{1+\nu}\left\{\frac{\partial^2 u}{\partial r^2} + \frac{\nu}{1-2\nu}\frac{\partial}{\partial r}\left[\frac{1}{r}\frac{\partial}{\partial r}(ru)\right] - \left(\frac{1+\nu}{1-2\nu}\right)\frac{dy_0}{dr}\right\} +$$

and:

$$\sigma_r\left(\frac{d}{dT}\log\frac{E}{1+\nu}\right)\frac{dT}{dr}.$$

$$\frac{\sigma_r - \sigma_\theta}{r} = \frac{E}{1+\nu}\left(\frac{1}{r}\frac{\partial u}{\partial r} - \frac{u}{r^2}\right).$$

Combining these:

$$\frac{\partial}{\partial r}\left\{\frac{1}{r}\frac{\partial}{\partial r}(ru) - \left(\frac{1+\nu}{1-\nu}\right)y_0\right\} = -\left(\frac{1+\nu}{1-\nu}\right)\left\{(1-2\nu)\frac{\sigma_r}{E}\gamma + y_0\mu\right\}\frac{dT}{dr}. \quad \text{(B14)}$$

where:

$$\gamma = \frac{d}{dT}\log G \qquad \mu = \frac{d}{dT}\log\left(\frac{1+\nu}{1-\nu}\right).$$

$G = E/2(1+\nu)$ being the shear modulus.

Zero-Order Solution

The usual approximation which neglects the variation of elastic moduli is obtained by placing the right side of Equation (B14) equal to zero. Denoting the radial displacement in this approximation by $u_0(r)$:

$$\frac{1}{r}\frac{\partial}{\partial r}(ru_0) = \left(\frac{1+\nu}{1-\nu}\right)y_0(r) + A_0. \quad \text{(B15)}$$

where A_0 is a constant. Strains corresponding to Equation (B15) are:

$$\epsilon_0 = \frac{u_0}{r} = \left(\frac{1+\nu}{1-\nu}\right)\frac{1}{r^2}\int_a^r y_0 r\,dr + \frac{A_0}{2} + \frac{B_0}{r^2}. \quad \text{(B16)}$$

$$\epsilon_r = \frac{\partial u_0}{\partial r} = \left(\frac{1+\nu}{1-\nu}\right)y_0 - \left(\frac{1+\nu}{1-\nu}\right)\frac{1}{r^2}\int_a^r y_0 r\,dr + \frac{A_0}{2} - \frac{B_0}{r^2}. \quad \text{(B17)}$$

The constants A_0 and B_0 will be determined from the condition that σ_r vanish at the inner and outer surfaces. The fact that the ends of the cylinder are free implies that $\bar{\sigma}_z = 0$, which leads to:

$$\epsilon_z = \frac{(1+\nu)(1-2\nu)}{(1-\nu)^2}\bar{y}_0 - \frac{\nu A_0}{1-\nu} . \tag{B18}$$

Insertion of the appropriate strains into Equation (B12) yields:

$$\sigma_r = \frac{E}{2(1-\nu)}\left\{A_0 + \frac{2\nu\bar{y}_0}{1-\nu} - \frac{2B_0(1-\nu)}{(1+\nu)r^2} - \frac{2}{r^2}\int_a^r y_0 r\,dr\right\}. \tag{B19}$$

The appropriate constants are:

$$A_0 = \frac{(1-3\nu)\bar{y}_0}{1-\nu} , \tag{B20}$$

$$B_0 = \frac{(1+\nu)a^2\bar{y}_0}{2(1-\nu)} , \tag{B21}$$

corresponding to:

$$\sigma_r = \frac{E}{(1-\nu)r^2}\int_a^r (\bar{y}_0 - y_0) r\,dr . \tag{B22}$$

First-Order Solution

The value of σ_r given by Equation (B22) may now be substituted into the right side of Equation (B14) and a new approximation obtained. We write: $u = u_0 + u_1$, where $u_0(r)$ is the displacement calculated above and given by Equation (B16), and $u_1(r)$ is the correction needed to take account of the variation of elastic moduli. Substituting into Equation (B14), keeping in mind the equation satisfied by u_0, leads to the following for u_1:

$$\frac{1}{r}\frac{\partial}{\partial r}(r u_1) = -\left(\frac{1+\nu}{1-\nu}\right)\left\{\frac{(1-2\nu)}{(1-\nu)}\int_a^r\left[\int_a^r (\bar{y}_0 - y_0) r\,dr\right]\left(\frac{dT}{dr}\right)\frac{dr}{r^2} + \mu\int_a^r y_0\left(\frac{dT}{dr}\right)dr\right\} + \text{const.} \tag{B23}$$

From this result we see that an equation like (B15) will hold for the new approximation for μ, provided $y_o(r)$ is replaced by:

$$y(r)=y_o(r)-\frac{(1-2\nu)\gamma}{1-\nu}\left\{\left[\int_a^r(\bar{y}_o-y_o)r\,dr\right]\left(\frac{dT}{dr}\right)\frac{dr}{r^2}-\mu\int_a^r y_o\left(\frac{dT}{dr}\right)dr\right. . \tag{B24}$$

Since the vanishing of σ_r at the inner and outer surfaces is to be maintained, $y(r)$ will replace $y_o(r)$ in expressions (B20) and (B21), giving new values to replace A_o and B_o. The corresponding approximation for σ_r is:

$$\sigma_r = \frac{E}{(1-\nu)r^2}\int_a^r(\bar{y}-y)r\,dr \quad . \tag{B25}$$

According to the radial equilibrium equation:

$$\sigma_\theta = \frac{d}{dr}(r\sigma_r) \quad . \tag{B26}$$

The circumferential stress corresponding to Equation (B25) is therefore:

$$\sigma_\theta=\frac{E}{1-\nu}\left\{(\bar{y}-y)-\frac{1}{r^2}\int_a^r(\bar{y}-y)r\,dr\right\}+r\sigma_r\frac{d}{dr}\log\left(\frac{E}{1-\nu}\right). \tag{B27}$$

At $r=b$, this reduces to:

$$\sigma_\theta(b)=\frac{E}{1-\nu}\left[\bar{y}-y(b)\right] \quad . \tag{B28}$$

Expression for the Maximum Power per Unit Length

It is now necessary to obtain a detailed form of Equation (B28) taking account of each of the several variations with temperature to first order. We begin by returning to the first integral on the right side of Equation (B24):

$$\int_a^r\left[\int_a^r(\bar{y}_o-y_o)r\,dr\right]\left(\frac{dT}{dr}\right)\frac{dr}{r^2} \quad .$$

Since this appears in a first-order correction term, it need be evaluated only to zero order. Thus:

$$\bar{y}_o - y_o = \alpha(\bar{T} - T) = \frac{\alpha Q}{2\pi K}\left(\left\langle \log\frac{b}{r}\right\rangle - \log\frac{b}{r}\right).$$

and:

$$\frac{dT}{dr} = \frac{-Q}{2\pi K r}.$$

The integral is:

$$\frac{-\alpha Q^2}{4\pi^2 K^2} J(r).$$

where:

$$J(r) = \int_a^r \left[\int_a^r \left(\left\langle \log\frac{b}{r}\right\rangle - \log\frac{b}{r}\right) r\, dr\right]\frac{dr}{r^3}. \qquad \text{(B29)}$$

or:

$$J(r) = \frac{1}{4}\left\{\left(\log\frac{r}{a}\right)^2 + \frac{b^2}{b^2-a^2}\log\frac{b}{a}\left(1 - \frac{a^2}{r^2} - 2\log\frac{r}{a}\right)\right\}. \qquad \text{(B30)}$$

Also:

$$\int_a^r y_o\left(\frac{dT}{dr}\right)dr = \alpha\int_{T_a}^{T}(T - T_b)\,dT = \frac{\alpha}{2}\left\{(T-T_b)^2 - (T_a - T_b)^2\right\}.$$

so that Equation (B24) becomes:

$$y(r) = y_o(r) + \frac{2\alpha Q^2(1-2\nu)}{4\pi^2 K^2(1-\nu)}\,J(r) - \frac{\mu\alpha}{2}\left\{(T-T_b)^2 - (T_a - T_b)^2\right\}.$$

Then, using Equation (B28):

$$\sigma_\theta(b) = \frac{E}{1-\nu}\left\{\bar{y}_o + \frac{2\alpha Q^2(1-2\nu)}{4\pi^2 K^2(1-\nu)}\left[\bar{J} - J(b)\right] - \frac{\mu\alpha}{2}\left\langle (T-T_b)^2\right\rangle\right\}. \qquad \text{(B31)}$$

The various expressions appearing in Equation (B31) can be readily developed further from earlier results. Thus, from Equation (B30):

$$\bar{J} - J(b) = \frac{1}{8}F\left(\frac{b}{a}\right). \qquad \text{(B32)}$$

where:

$$F(x) = 1 + \frac{2\log x}{x^2-1} - \frac{2(1+3x^2)}{(x^2-1)^2}(\log x)^2 \quad . \tag{B33}$$

Also:

$$\langle (T-T_b)^2 \rangle = \frac{Q^2}{4\pi^2 K^2} \left\langle \left(\log \frac{b}{r}\right)^2 \right\rangle \quad . \tag{B34}$$

Further, for a linear variation of α with temperature:

$$\alpha = \alpha_b \left[1 + \beta (T - T_b) \right] \quad , \tag{B35}$$

$y_o(r)$ takes the form:

$$y_o = \alpha_b \left\{ (T-T_b) + \frac{\beta}{2}(T-T_b)^2 \right\} \quad . \tag{B36}$$

Then, using Equation (B9), one obtains to first order in β and λ:

$$\overline{y_o} = \frac{Q\alpha_b}{2\pi K_b} \left\langle \log \frac{b}{r} \right\rangle \left\{ 1 + \frac{Q(\beta-\lambda)}{4\pi K_b} \frac{\left\langle \left(\log \frac{b}{r}\right)^2 \right\rangle}{\left\langle \log \frac{b}{r} \right\rangle} \right\} . \tag{B37}$$

When Equations (B32), (B34), and (B37) are inserted into (B31), the expression for $\sigma_\theta(b)$ becomes:

$$\sigma_\theta(b) = \frac{EQ\alpha_b \left\langle \log \frac{b}{r} \right\rangle}{2\pi K_b (1-\nu)} \left\{ 1 + \frac{Q}{16\pi K_b \left\langle \log \frac{b}{r} \right\rangle} \left[4(\beta-\lambda-\mu) \left\langle \left(\log \frac{b}{r}\right)^2 \right\rangle + \gamma \left(\frac{1-2\nu}{1-\nu}\right) F\left(\frac{b}{a}\right) \right] \right\} . \tag{B38}$$

The corresponding maximum power per unit length is

$$Q_{max} = \frac{2\pi K_b (1-\nu) P}{E\alpha_b \left\langle \log \frac{b}{r} \right\rangle} (1-\delta) \quad , \tag{B39}$$

where:

$$\delta = \frac{(1-\nu)P}{8E\alpha_b \left\langle \log \frac{b}{r} \right\rangle^2} \left\{ 4(\beta-\lambda-\mu) \left\langle \left(\log \frac{b}{r}\right)^2 \right\rangle + \gamma \left(\frac{1-2\nu}{1-\nu}\right) F\left(\frac{b}{a}\right) \right\} . \tag{B40}$$

Equation (B39) should be compared with (B2), keeping in mind the value of $\left\langle \log \frac{b}{r} \right\rangle$ as given by (B10). The new equation differs from the

old only by the factor $(1-\delta)$. The usual approximation is valid if δ is negligibly small. No careful test has been made in any specific case, partly because information on the temperature variation of elastic moduli is not available. A rough check in the case of one BeO cylinder, using plausible values for the constants, led to δ of order 1%.

APPENDIX C

Apparatus and Procedures

Thermal-Rupture Apparatus

The thermal-rupture apparatus was designed to provide a controlled heat flow through the wall of a hollow, tubular specimen. Although several design modifications were incorporated, its operating principle was the same as that of equipment built or planned for thermal-rupture work at Oak Ridge and Argonne National Laboratories, and discussed in MonN-383, ORNL-22, ORNL-66, and ETL-12.

Figure 1 is a schematic drawing of the apparatus with a specimen in place. Heat is generated in a graphite resistor rod mounted vertically in an evacuated chamber having water-cooled walls. The specimen is aligned concentrically on the heater rod at approximately midspan. Guard tubes, similar to the specimen, are aligned above and below the specimen so that the full effective (reduced) length of the heater rod is surrounded. The primary function of the guard tubes is to reduce axial heat flow in the specimen and in the center, "gauge" section of the heater rod. The lower guard tubes, of course, also support the specimen.

Concentric alignment of the tubular column on the heater rod is accomplished by split washer-like, spacer rings placed between the specimen and guard tubes. The spacer rings fit the heater rod and have shoulders to prevent lateral movement of the specimen or guard tube.

Experiments on establishing the proper design and material for guard tubes and spacer rings are covered later in this Appendix.

In addition to the guard tubes, two other design measures are taken in the interests of providing only radial heat flow to, and in, the specimen. The heater rod is considerably longer than the specimen, thus minimizing the axial temperature gradient caused by conduction in the rod. The other measure consists of using uncooled graphite discs as shields to reduce radiation to the cooled end surfaces of the chamber.

The top and sides of the chamber form a can of double-wall construction. Cooling water, circulated between the walls, enters the can at 8 points on the bottom from a single header. A single discharge is provided for the water in the top of the can. There are four small windows in the can for viewing the specimen. Three of these windows are spaced 120° apart on a circumference on a level with the center of the specimen. The fourth window is located slightly above the plane of the other three windows. With this arrangement, an optical pyrometer can be used in a fixed installation while all points on a periphery of the specimen are under visual observation. A windlass and cable is provided for raising and lowering the can on four vertical guide rods.

In the lowered position, the can rests on an "O" ring which provides a vacuum seal between the can and base. A double-circulating water system cools the base. Four insulated terminals extend through the base to permit taking voltage readings inside the chamber, or to make other desired electrical connections between the inside and outside of the chamber. Also, provisions are made for evacuating the chamber through the base.

The top electrical connection to the graphite heater rod is through an interchangeable tapered fitting attached to the top of the can. An enlarged tapered end on the graphite rod engages the fitting when the

can is lowered. The bottom of the heater rod also is enlarged and extends through the base. A vertical copper rod screws into the lower end of the heater rod for the bottom electrical connection. The rod rests on a plate which, in turn, rests on two springs suspended from the base of the chamber. This arrangement provides a flexible and adjustable support for the heater rod. It permits alignment of the rod for proper seating in the taper joint when the can is lowered and, after seating, the rod can adjust itself, by vertical movement on the springs, to compensate for length changes caused by heat or pressure. A Wilson-type vacuum seal around the copper rod allows such vertical movement of the heater rod. The Wilson seal is mounted on a flexible, double-Sylphon support. The annular space between the Sylphons serves as a water jacket for cooling the lower end of the heater rod and associated parts.

Operation in a vacuum prevents convection currents, hence reduces axial heat flow in the specimen, as well as protecting the graphite heater rod against oxidation. For evacuating the chamber, a mechanical pump is supplemented, at low pressures, by an oil booster pump. A Pirani gauge indicates when the vacuum reaches a safe operating level. The gauge has not been calibrated, but, from manometer readings, a pressure of about 1000 microns exists when the Pirani gauge first begins to indicate. Trials have shown that pressures as low as 20 microns can be obtained with this type of pumping system, and there have been no indications of heater rods oxidizing to date.

A 1000-ampere welding transformer furnishes power for the apparatus. The transformer is of the adjustable-current type, with the voltage remaining approximately constant. The transformer primary operates on

220 volts, single phase, through a line fused at 400 amperes. It is equipped with a motor control to increase or decrease the secondary current output.

The amount of power dissipated per unit length of the portion of the heater rod opposite the specimen is determined by current and voltage measurements. With only radial heat flow, this is the amount of heat per unit length that passes through the specimen wall. To measure the voltage, two small holes are drilled, to a depth of about 3/16 inch, near each end of the gauge section of the heater rod. The distance between these holes is measured accurately. A 6-mil tungsten wire is forced into each hole, and passed through a small hole drilled in a guard tube. Two of the terminals extending through the base are used to make connections with the tungsten wire. The voltage drop is measured with an electronic AC volt meter, which is relatively unaffected by high resistance in the electrical circuit.

The current flowing through the heater circuit is measured by an ammeter connected to a coil around one of the current leads inside the transformer case.

The product of this current and the voltage drop, divided by the distance between the wire connections on the heater rod, is the power dissipated per unit length of heater rod at the "gauge" section.

The apparatus is designed to be quite versatile. Various-sized specimens, both as to length and radius, can be tested. Also, some variation undoubtedly could be made in the geometry of the cross section of the single-holed tubes used for specimens. All tests to date, however, have been on tubes with circular cross sections. With a given specimen,

the power per unit length required to reach a certain mean wall temperature conceivably could be varied without much trouble, by changing the character or temperature of the inner wall of the chamber. No such variations have been made as yet. A dull, black sulfide coating was applied to the chamber wall when the apparatus was built.

Testing Procedure

To begin a test, the can is raised to its top position, permitting ready access, and the specimen, guard tubes, spacer rings, graphite-disc shields, and voltmeter leads are assembled on the heater rod. With the Wilson seal and heater-rod support loosened, the can is then gently lowered, taking care to insure that the heater rod enters the top, taper joint properly. Next, the heater-rod support is tightened, and the Wilson seal is partially tightened. The mechanical pump is then started. After the pressure is significantly reduced, the Wilson seal is fully tightened. When the pressure is low enough for the Pirani gauge to give a reading, the booster pump is started and, after the Pirani-gauge readings become constant, the cooling water is turned on.

As the next step, current is applied to the heater rod in increments. The initial load, of course, must be below that required to fracture the specimen. As the critical stress at a given power builds up during the transient-state conditions to a maximum under steady-state conditions, "thermal shock" is of no particular concern. However, care must be taken to insure that steady-state conditions are attained during each power increment. This is accomplished by holding the power at each level until the outer-wall temperature of the specimen is constant, as

indicated by readings of the optical pyrometer. This temperature and the corresponding voltmeter and ammeter readings are recorded. These electrical data and the distance between voltmeter leads on the heater are used to indicate radial heat flow through the specimen, as mentioned earlier. After the initial load is applied, each increment usually is of the order of 2 watts per cm. Approximately 3 minutes is required for the outer-wall temperature to become constant for each of these increments.

No difficulty has been encountered to date in detecting fracture of the specimen. There is a sudden appearance of one or more full-length, longitudinal cracks, exposing the heater rod and flooding the chamber with light. Voltmeter, ammeter, and outer-wall-temperature readings at fracture, of course, are recorded.

After fracture of the specimen, the current is turned off, and the system allowed to cool. The pumps and cooling water are then turned off, and air admitted. Again, the Wilson seal and heater-rod support are loosened, followed by raising the can and removing the broken specimen.

With two trained operators and a general knowledge of the thermal-rupture behavior of the specimen, a test cycle, such as described here, requires about 3 to 4 hours.

Experiments with Spacer Rings

Previously, in describing the thermal-rupture apparatus, it was pointed out that spacer rings were used to effect concentric alignment of the specimen and guard tubes on the heater rod. These rings are shown in place in Figure 1.

As the spacer rings must touch both the heater rod and specimen, some heat is transferred through them by conduction. Also, their location, in the annulus between heater rod and specimen, influences radiant heat transfer in the system. These factors require consideration before it is safe to assume only radial heat flow to and in the specimen. Along this line, in measuring heat flow, it is assumed that all of the heat generated in that portion of the heater rod opposite the specimen is transferred uniformly to the inner wall of the specimen. Also, in calculating thermal stress, it is assumed that this heat proceeds along a direct radial path to the outer wall of the specimen.

If this picture of heat transfer is affected significantly by the presence and nature of the spacer rings, one might expect an appreciable change in the thermal stress in a specimen with changes in the spacer rings. Such changes in stress, of course, would be reflected in the measured power per unit length at fracture.

Accordingly, several series of thermal-rupture tests were conducted with the presence and nature of the spacer rings as the only variable in each series. When no spacer rings were used, the specimen and guard tubes were aligned with extreme care, and attention was given to insuring that the joints were tight and smooth. In tests using spacer rings, three variations were made in design and two in material. The different designs are shown in Figure 10. The rings were machined from either a porous alumina brick (Norton Company's No. 1099) or from a graphite block.

Tubular specimens of the sintered-ruby body were used. They had circular cross sections 7/8 in. ID x 1-5/16 in. OD. The spacer rings,

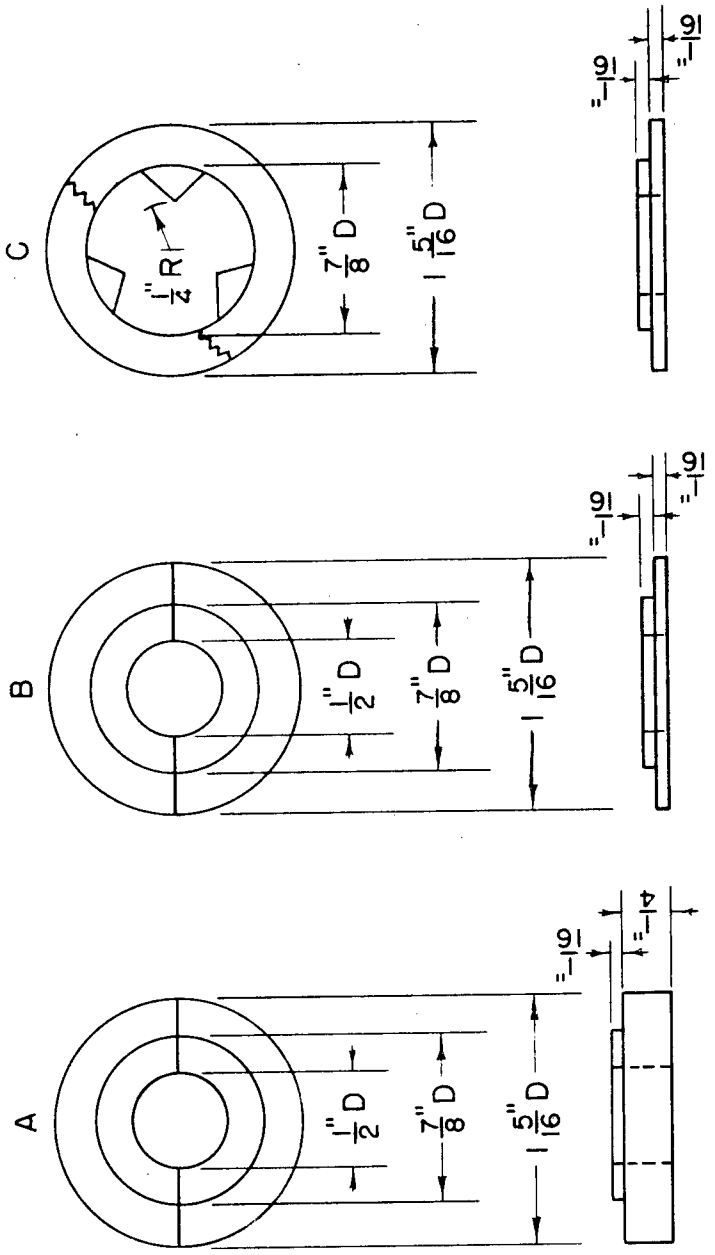

FIGURE 10. SPACER-RING DESIGNS

of course, were dimensioned so as to fit these specimens and the particular heater rod used; hence, the spacer-ring dimensions given in Figure 10 would not be generally applicable for all assemblies.

One series of experiments indicated that changing the design of alumina spacers from that of "A" to "B" in Figure 10 had no appreciable effect. A change from alumina to graphite, using design "B", however, resulted in fracture at a considerably higher power per unit length. In other words, the stress for a given heat flow apparently was lowered by substituting graphite for alumina in the spacers. The data were as follows:

Specimen Number	Spacer Ring		Power Per Unit Length at Fracture, watts/cm	Outer-Wall Temperature at Fracture**, F
	Design*	Material		
17N	A	Alumina	65	1600
18N	A	"	66	1640
19N	A	"	65	1645
20N	B	"	66	1620
21N	B	"	67	1620
23N	B	Graphite	88	1730
24N	B	"	93	1735

Another series of tests supported this indication that graphite spacers cause an increase in the power per unit length at fracture. Using the "A" design, six specimens broke at an average of 58 watts/cm, with the maximum of 62 watts/cm, when alumina was used in the spacers. But when a graphite spacer was used in a single test, the specimen broke at 71 watts/cm. The ruby specimens for this series were 2 inches long, while 1-inch specimens were used in the previous series.

---

* The designations, "A" and "B", were taken from Figure 10.

** Uncorrected, optical-pyrometer reading.

In still another series of tests, the results were about the same when alumina spacer rings were used as when the specimens and guard tubes were aligned, with extreme care, without using spacer rings. Ruby specimens 4 inches long were used. The data were as follows:

Specimen Number	Spacer Ring Design*	Spacer Ring Material	Power Per Unit Length at Fracture, watts/cm	Outer-Wall Temperature at Fracture**, F
2-32-1	A	Alumina	60	1610
-2	A	"	59	1675
-3	A	"	63	1585
-4	--	--	57	1600
-5	--	--	62	1610

Finally, a series of tests were conducted to compare the use of graphite spacers of design "C" with the spacer-free assembly. Specimens 4 inches long were again used, and the following data were obtained:

Spacer Ring Design***	Spacer Ring Material	Number of Specimens Tested	Average Power Per Unit Length at Fracture, watts/cm	Standard Deviation, watts/cm	Average Outer-Wall Temperature at Fracture****, F
C	Graphite	6	55	2.6	1590
--	--	10	53	4.7	1570

Considering all of the series of tests, it is concluded that spacers affect the power needed to cause fracture only if they permit high heat flow by conduction from the heater rod to the ends of the

---

* The designation, "A", was taken from Figure 10.

** Uncorrected, optical-pyrometer reading.

*** The designation, "C", was taken from Figure 10.

**** Uncorrected, optical-pyrometer reading.

specimen. The use of porous alumina spacers of either design "A" or "B", or of graphite spacers of design "C", or the use of a spacer-free assembly, all provide poor thermal contact, and they all performed about alike. On the other hand, when better thermal contact was provided by graphite spacers of design "A" or "B", the power for fracture was increased. Further, in view of the several variations, it might be assumed that axial heat flow was negligible from the use of all methods which provided poor thermal contact.

Although the spacers were too thin for optical-pyrometer readings, brightness observations during tests indicated that the outer surface of graphite spacers ran hotter than that of the specimen, as expected. An opposite effect was noted when alumina spacers were used. This, of course, would mean a longitudinal temperature difference between the center and ends of the specimens, dependent in character on the material used for spacers. From the results of tests with variations in spacers, apparently such axial temperature differences did not appreciably influence the critical stress when the spacers provided poor thermal contact between the heater rod and specimen.

With the ends of specimens hotter than their midsections when the graphite spacers of designs "A" or "B" were used, a higher power per unit length should be required for fracture. as observed. The circumferential thermal expansion would tend to be greatest at the ends. The restraint imposed by neighboring cross sections which have expanded less would produce a tangential compressive stress. This stress opposes the tangential tensile stress produced in the outer fibers by the radial heat flow. As this tangential tensile stress is critical at the ends, a

higher radial heat flow (power) is required for fracture here than in the case where there is no axial heat flow.

Cursory experiments indicated that seizure at the contact surfaces of spacer rings and specimen did not effect the stress system. Fracture occurred at essentially the same power per unit length when contact surfaces of alumina spacers were "greased" with graphite as in otherwise similar tests with unlubricated surfaces.

Unless otherwise specified, graphite spacer rings of design "C", or their equivalent, were used to obtain data for all studies covered in this report. These particular spacers were especially adaptable because of the easy machinability of graphite.

Experiments with Guard Tubes

The nature of the guard tubes also affects the heat transfer in the system, hence, the thermal stress in a specimen. Accordingly, as in the study of spacer rings, controlled thermal-rupture tests were made using two different types of guard tubes.

The main purpose of the guard tubes is to prevent axial heat flow in the specimen. If the guard-tube temperature depended only on radial heat flow, one would obviously use the same material and cross section as the specimen in guard tubes. However, the guard tubes separate the specimen from the cooler ends of the chamber. Low thermal conductance in guard tubes, therefore, appears desirable to reduce axial heat flow.

For these reasons, consideration was limited in the experimental work to guard tubes either of low conductance or of the same material and cross section as the specimen. As in the spacer-ring studies,

sintered-ruby tubes of circular cross section, 7/8 in. ID x 1-5/16 in. OD, were used for specimens. Thin-walled construction and a low-conductivity material were used in the low-conductance guard tubes. They were prepared of a porous sintered zircon*, having a thermal conductivity approximated to be less than one-third that of the sintered ruby, and had walls about one-half as thick as those of the ruby tubes. The comparative data from fracturing tubes 2 inches long were as follows:

Guard Tubes	Number of Specimens Tested	Average Power Per Unit Length at Fracture, watts/cm	Standard Deviation, watts/cm	Average Outer-Wall Temperature at Fracture, F
Zircon	6	58	5.0	1550
Ruby	4	57	2.6	1560

In another series of more cursory tests, using specimens 4 inches long, the agreement was less conclusive. Two specimens were tested using zircon guard tubes. They failed at 60 and 57 watts/cm, while 6 specimens fractured at an average of 55 watts/cm when ruby guard tubes were used under otherwise similar conditions.

As might be expected, brightness observations during tests indicated that the zircon guard tubes ran much cooler than the specimen, while the ruby guard tubes and specimen maintained about the same temperature. These observations deny the remote possibility of a difference in emissivity between the zircon and ruby equalizing the effect of the difference in conductance of the two types of guard tubes.

From these results, it appears that the critical thermal stress in the present test is not affected significantly by axial heat flow.

---

* Their true porosity was 24 per cent.

Lowering the conductance of the guard tubes by more than a factor of 6 had little effect on the power per unit length at fracture. Such a change certainly lowered the axial heat flow to the ends of the chamber. The assumption that stresses in the specimen are from only radial flow seems valid from the standpoint of any guard-tube effects.